Hypersonic Boundary-Layer Transition over a Blunt Circular Cone in a Mach 8 Digital Wind Tunnel

Mateus Schuabb, and **Lian Duan**
The Ohio State University, Columbus, OH 43210
Anton Scholten
North Carolina State University, Raleigh, NC 27695
Pedro Paredes
National Institute of Aerospace, Hampton, VA 23666
Meelan M. Choudhari
NASA Langley Research Center, Hampton, VA 23681

Supported by ONR

Background

Disturbance Environment for High-Speed Wind-Tunnel Facilities

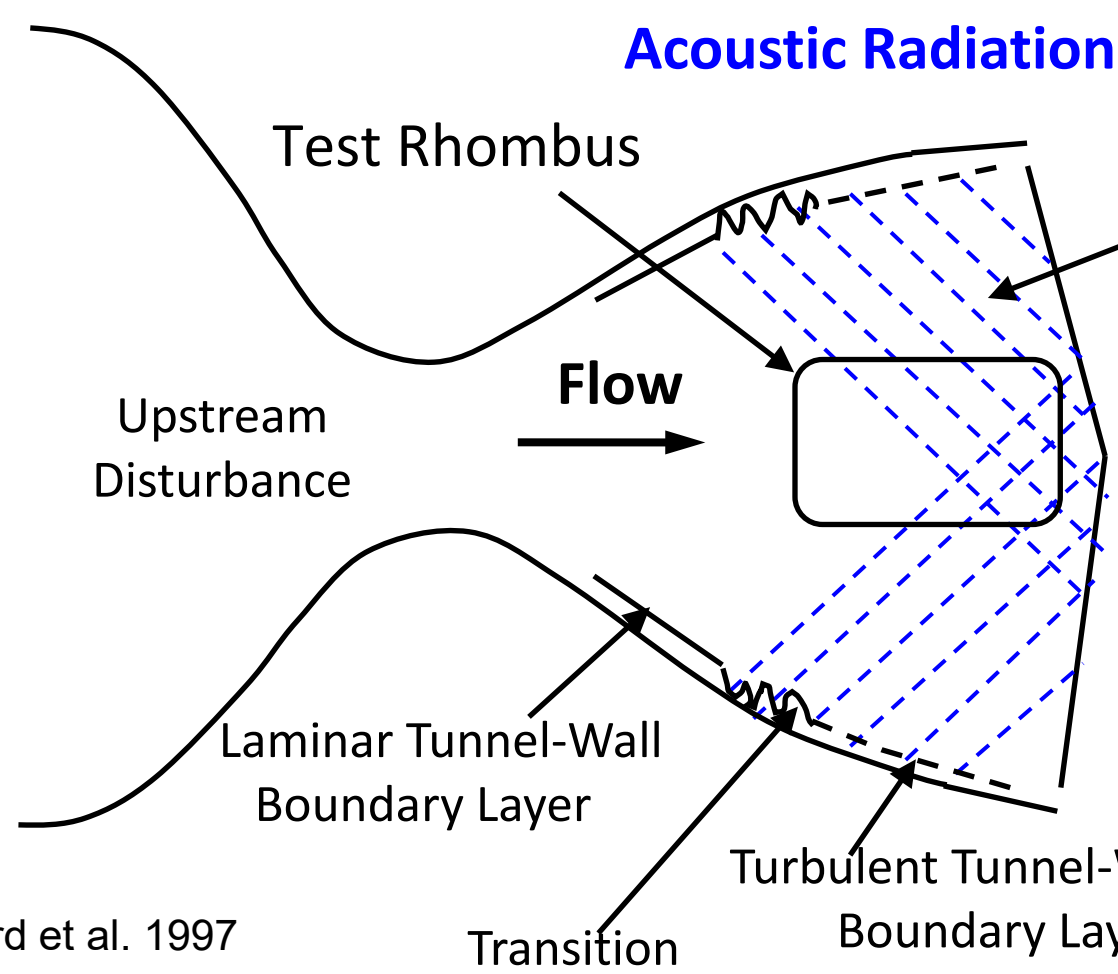

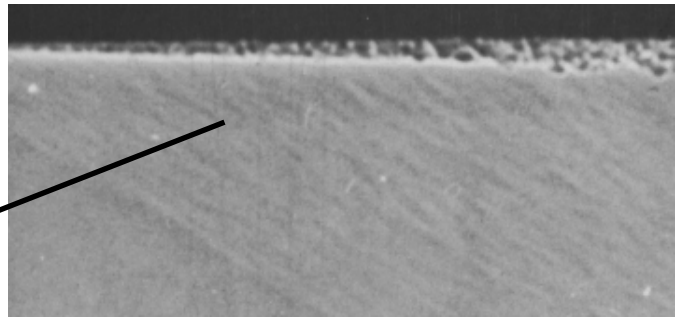

Shadowgraph of the radiated noise from a Mach 3.5 tunnel-wall turbulent boundary layer (courtesy of NASA Langley)

In a conventional tunnel ($M_\infty > 2.5$), tunnel noise is dominated by acoustic radiation from turbulent boundary layers on tunnel side-walls (*Laufer, 1964*)

Methodology

Mimic the transition process in the tunnel-like environment

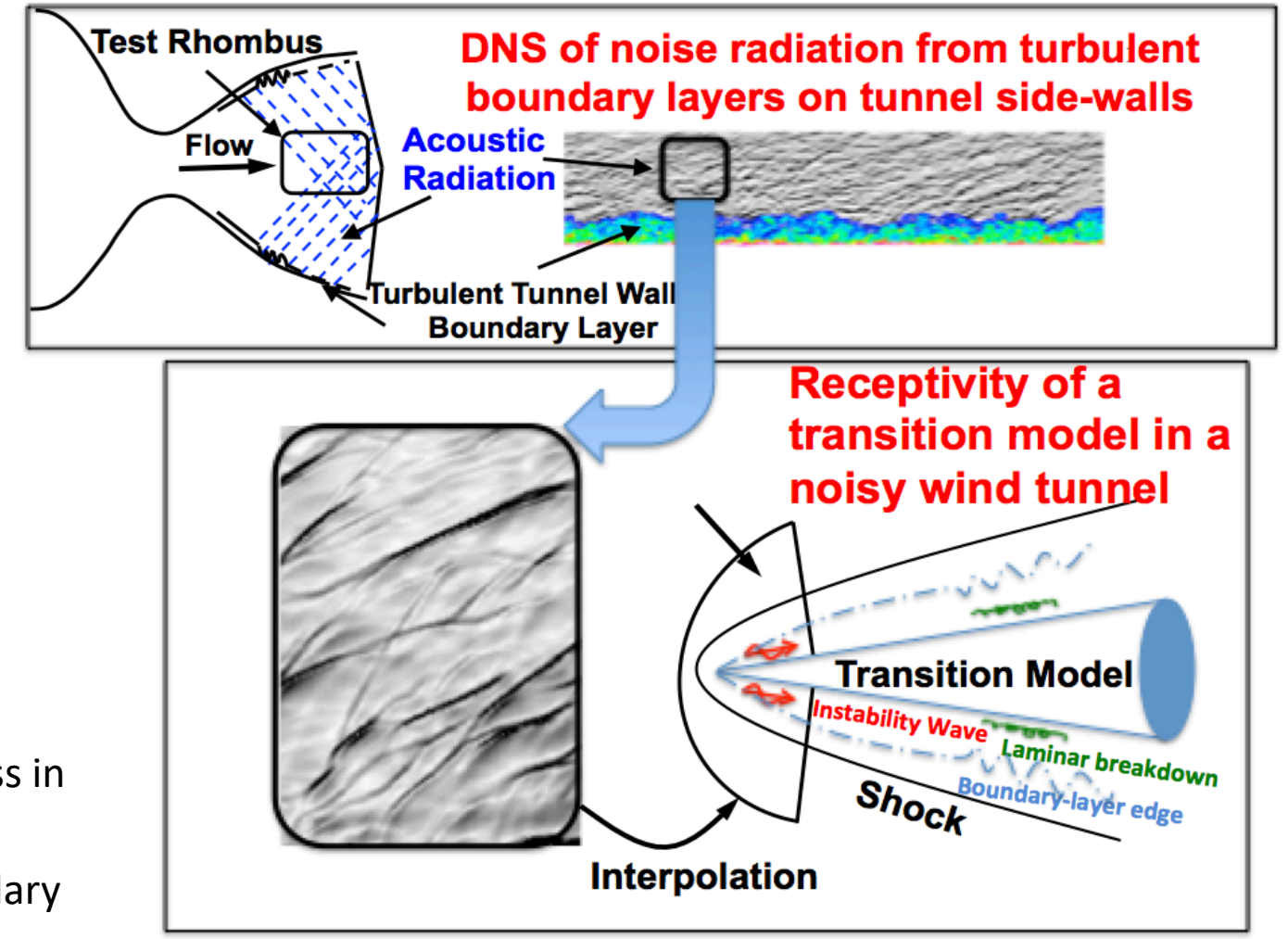

Freestream disturbances:

- Precursor DNS of Full-scale Nozzle of Sandia HWT-8
- Characterization of the acoustics radiation from turbulent boundary layer of the wind tunnel walls
- These acoustics disturbances were imposed at the freestream boundary conditions for the DNS

Potential contributions:

- Generate improved knowledge of receptivity process in facility-disturbance environment
- Provide the initial disturbances in hypersonic boundary layers required for conducting stability analysis
- Help to understand the transition reversal phenomenon

"Tunnel-like" Acoustic Disturbance Generation

- Instantaneous acoustic structures of the modeled acoustic disturbances matched well with those computed by DNS

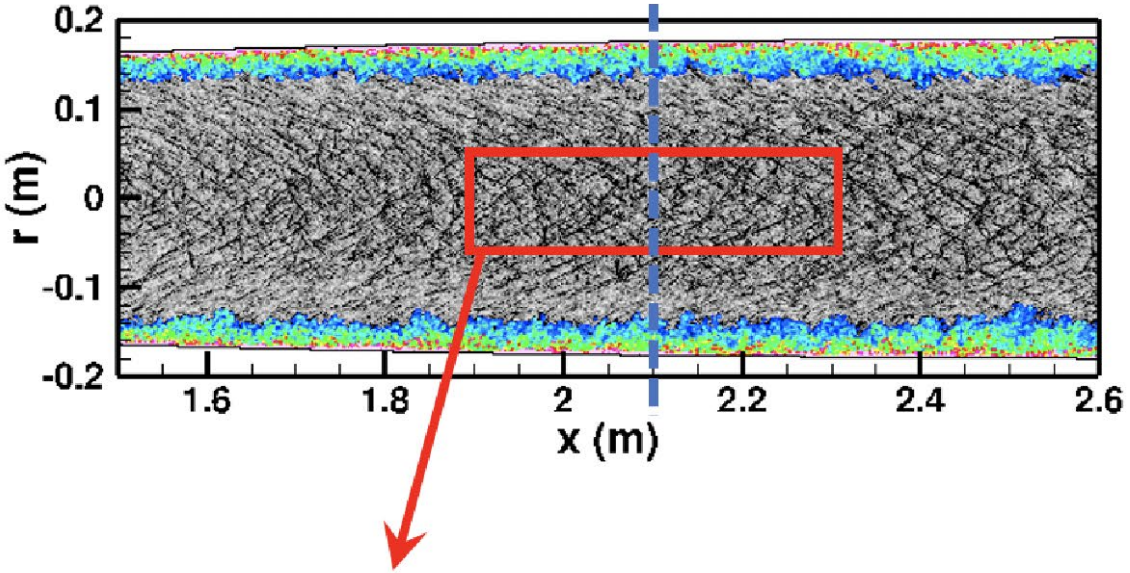

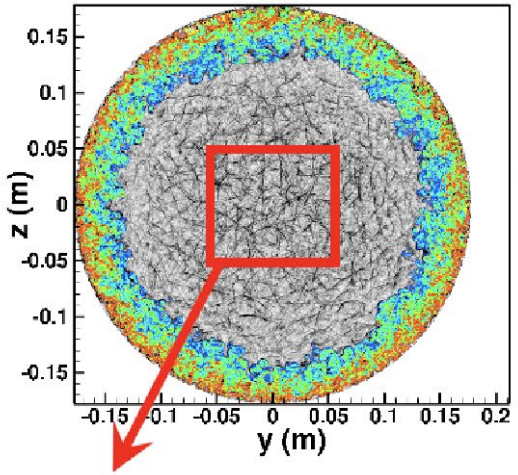

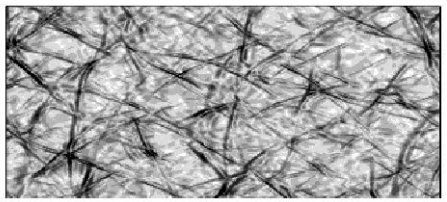

DNS (x-r plane)

extract
reconstruct

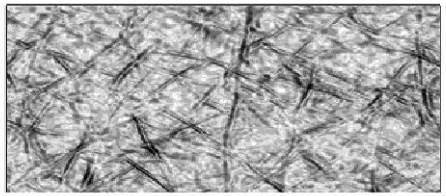

Acoustic Model (x-r plane)

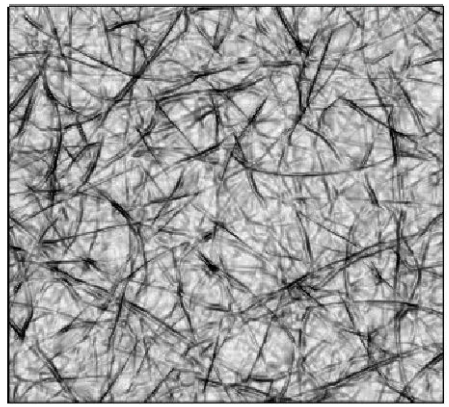

DNS (y-z plane)

extract
reconstruct

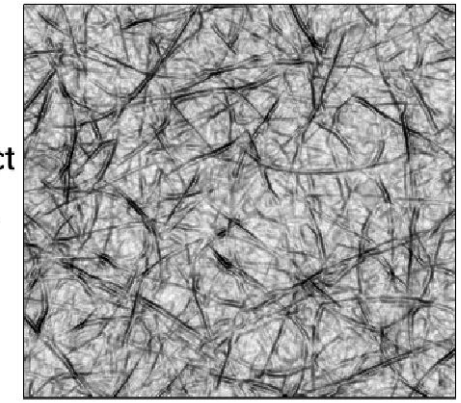

Acoustic Model (y-z plane)

"Tunnel-like" Acoustic Disturbance Generation

- Power Spectral Density (left):
  - Very good agreement between slow-acoustic-wave assumption and the precursor nozzle-DNS data
  - Reconfirming the dominance of slow acoustic waves

- The wavenumber spectra in x, y, and z direction (bottom):
  - The model results matched very well with those computed by the wind-tunnel nozzle DNS

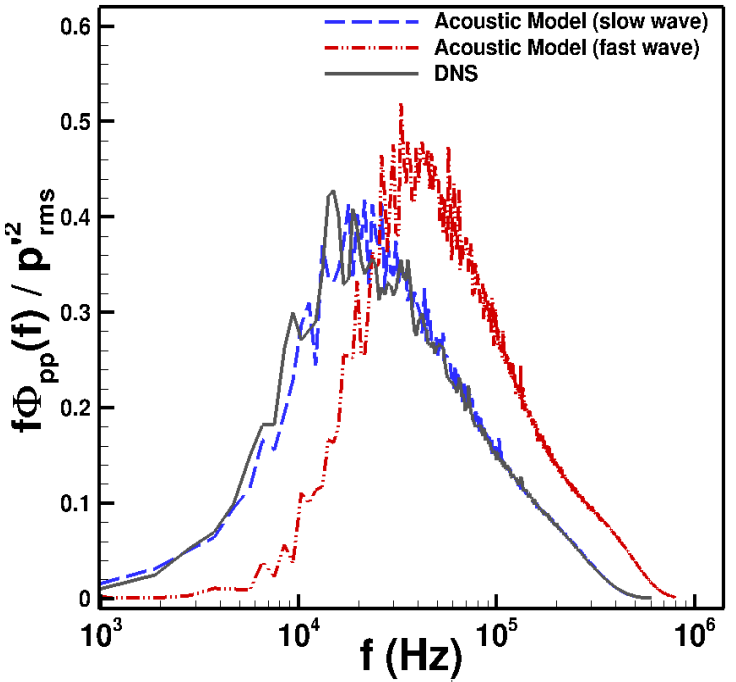

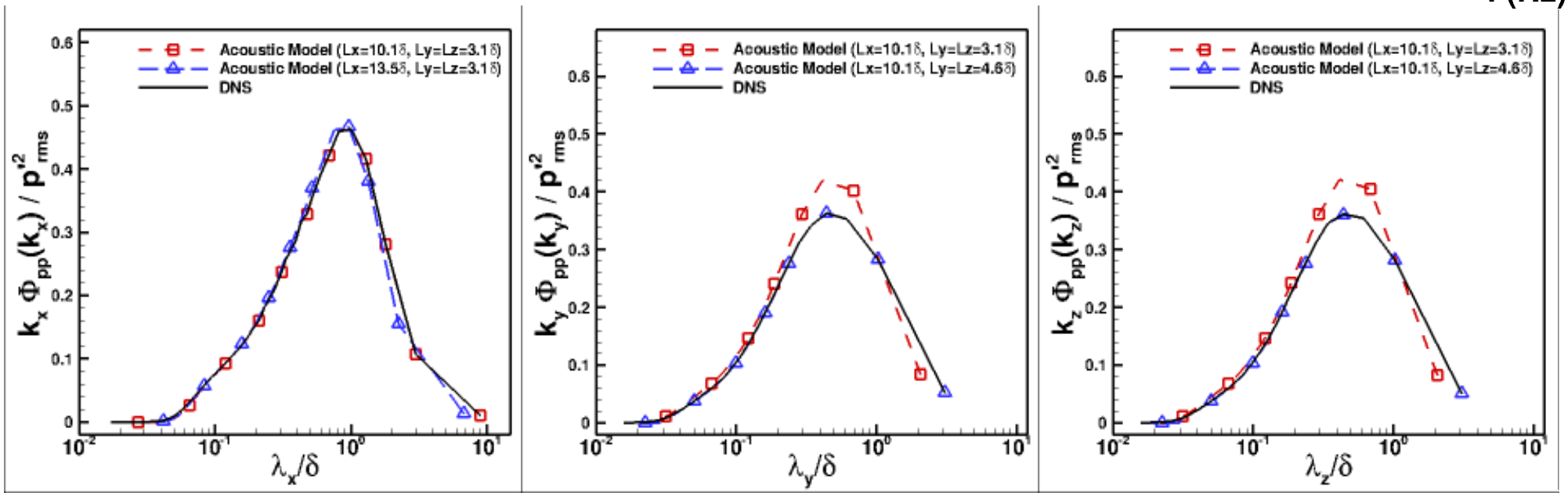

"Tunnel-like" Acoustic Disturbance Generation

- Apparent similarity in the evolution of the instantaneous acoustic structures between the model and DNS
- Stochasticity of the freestream acoustic field very well preserved by the model

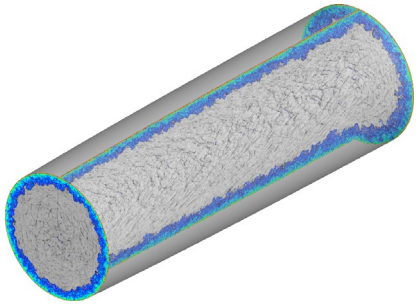

DNS of Acoustic Disturbances in Sandia HWT-8

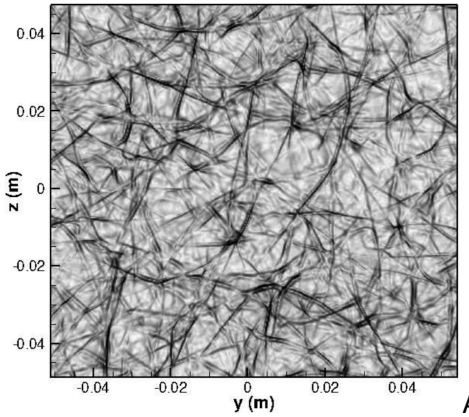

t = 0

DNS

Acoustic model

t = 17.4 μs (3 Λ)

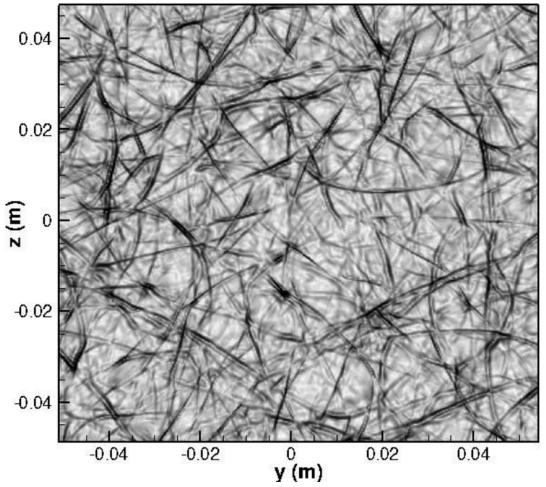

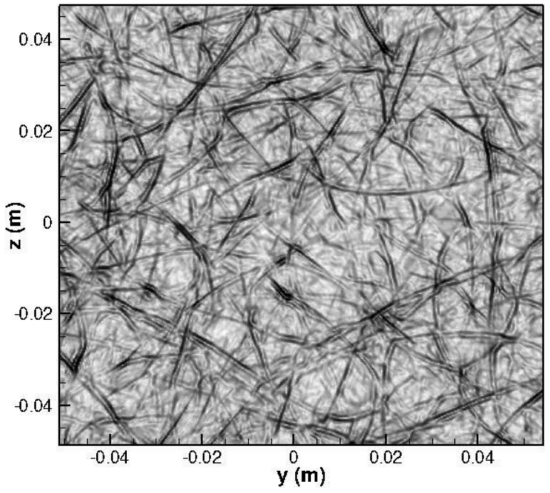

t = 52.2 μs (9 Λ)

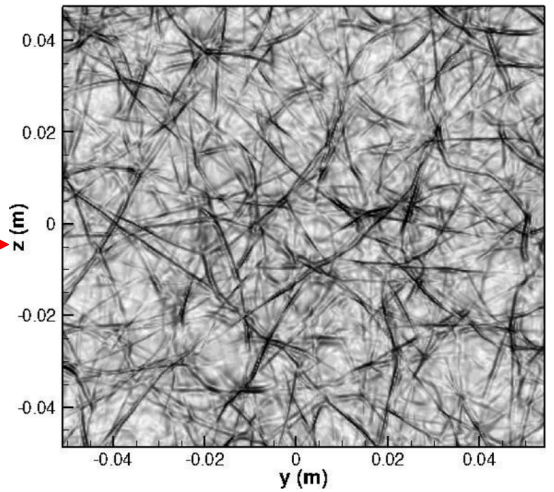

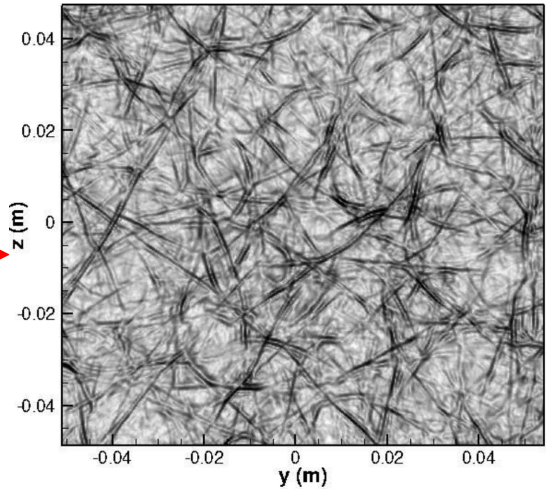

DNS

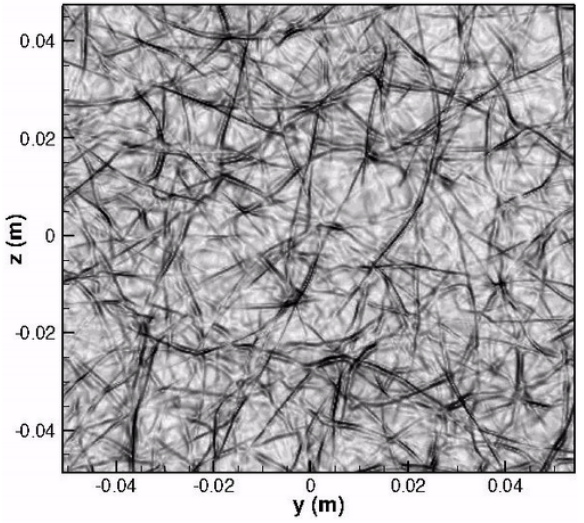

Acoustic model

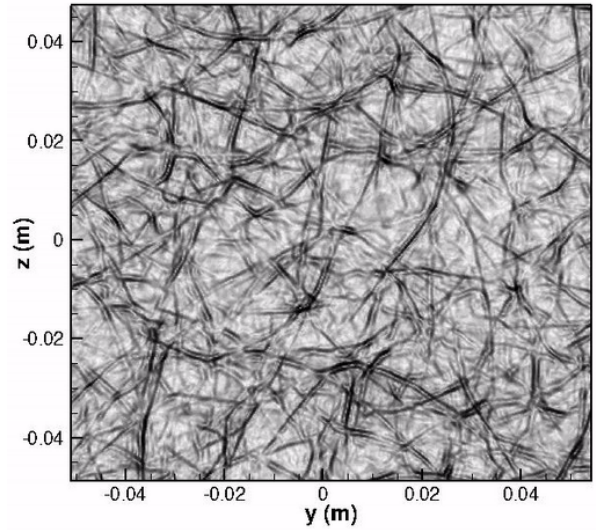

Motivation and Objectives

- Improve our previous simulation results of **Liu et al. (2022)**
  - Eliminated numerical noise generated at the curved strong shock
  - Added an azimuthal spectral filter applied at x ≈ 0.11 m
- Compute the results for longer times and longer length of the cone
  - The simulation time is extended from t_f ≈ 0.48 ms to t_f ≈ 0.58 ms (an increase of approximately 20%)
  - Converged results until x ≈ 0.55 m, in comparison with x ≈ 0.45 m
- More detailed data analysis
  - Frequency spectrum as a function of x
  - Frequency and azimuthal wavenumber spectrum as a function of wall-normal direction
  - Extraction of Fourier modes from fluctuations field

Liu et al. (2022)

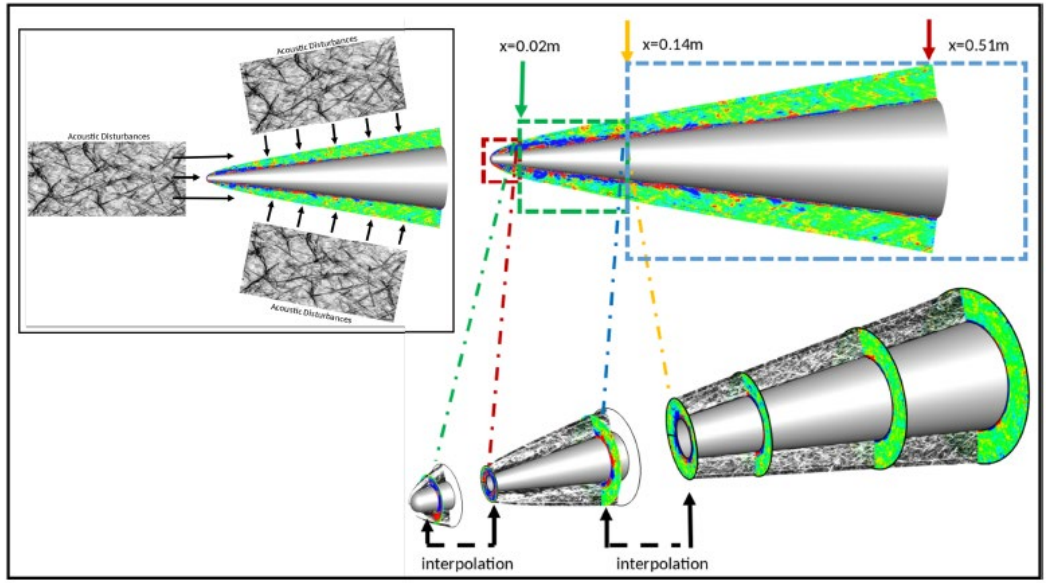

Present Work

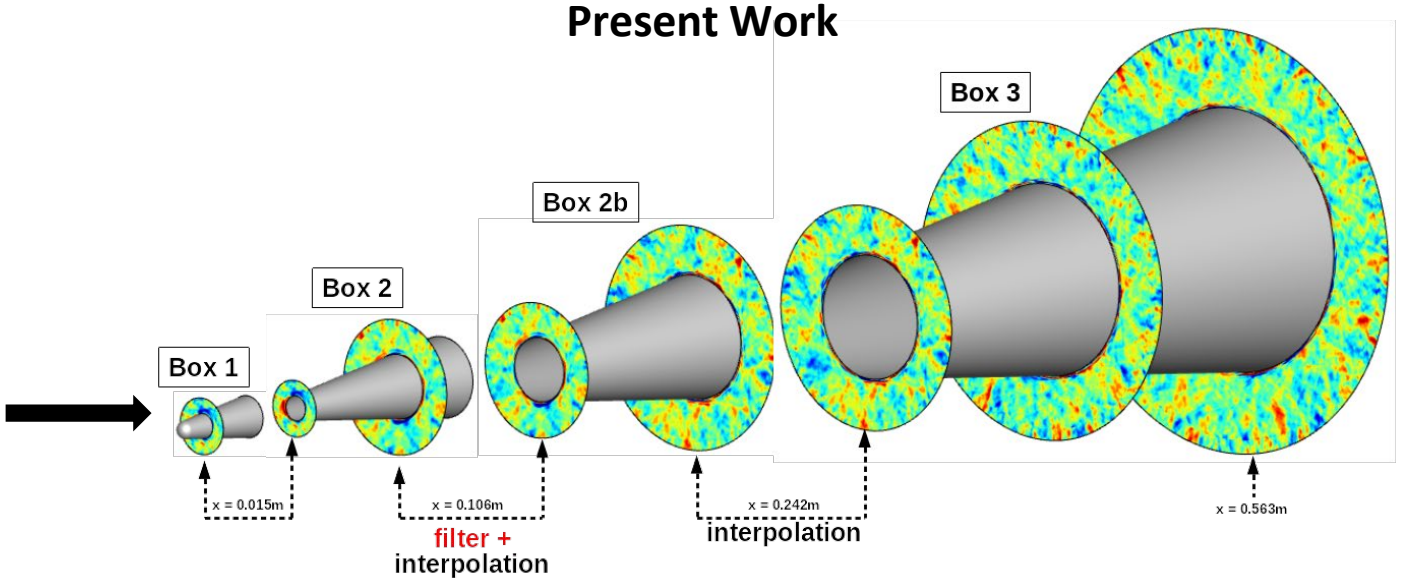

Numerical Setup

- 7° half-angle cone (R_n = 5.2mm) at Mach 8
- The domain is divided into 4 subdomains
- Tunnel-like acoustic disturbances are imposed at all freestream boundary
- Interpolation is performed at the inlet of downstream boxes
- The filter is applied at the inlet of box 2b
- WENO7 is used for the convective terms
- Fourth-order central scheme for viscous terms
- Third-order low-storage Runge-Kutta scheme

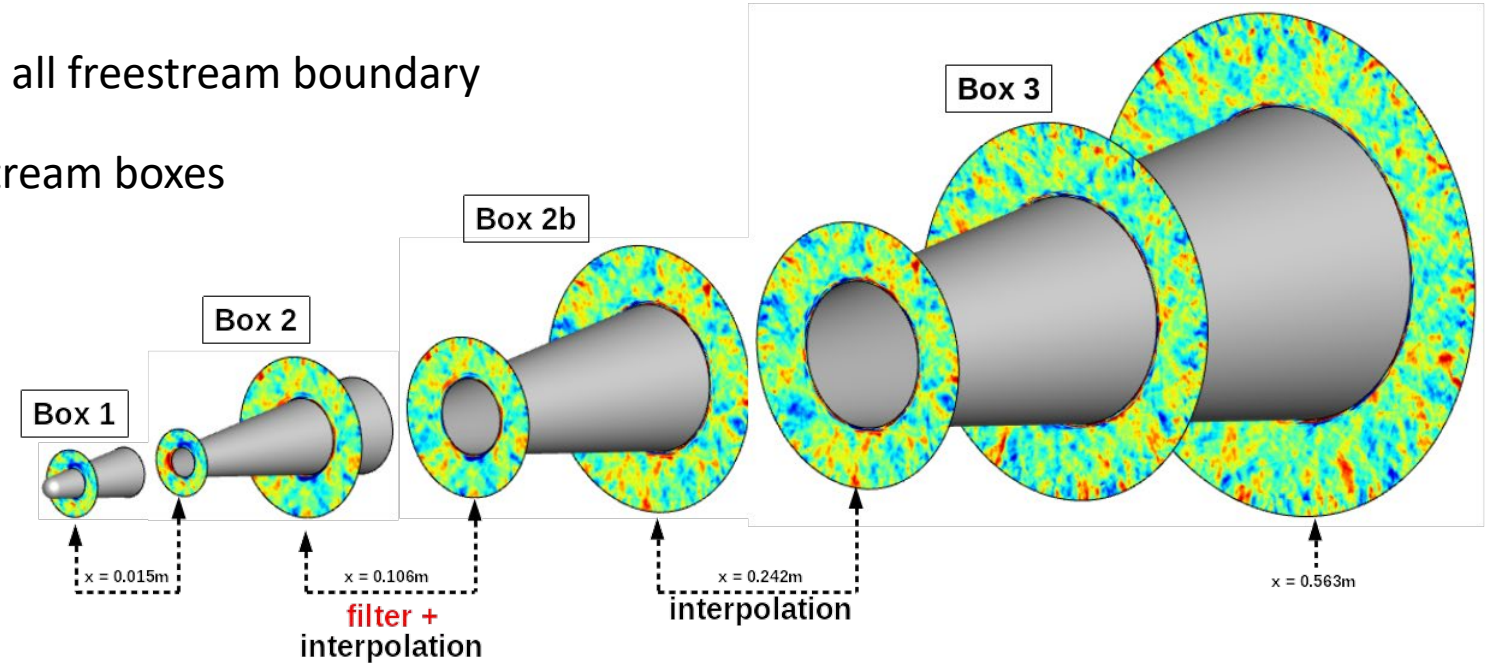

Case	N_x x N_θ x N_r	x (m)	Δx^+	$(R\Delta\theta)_w^+$	Δr_w^+	Δt (s)
Box 1	2800 x 256 x 1440	-0.0061 - 0.02	0.23 – 0.23	0.003 – 4.28	0.01 – 0.11	1.6534392e-10
Box 2	1050 x 256 x 1440	0.015 - 0.144	0.23 – 4.72	4.18 – 13.46	0.10 – 0.27	1.98412698e-9
Box 2b	2100 x 512 x 1440	0.106 - 0.252	4.72 – 4.72	5.34 – 10.58	0.23 – 0.34	7.93650794e-9
Box 3	1800 x 1024 x 1440	0.242 - 0.563	4.72 – 4.72	5.12 – 10.89	0.34 – 0.34	7.93650794e-9

Normalized by viscous length $z_\tau \approx 41\ \mu m$ at x = 0.3 m

Results: Wall Statistics

- Comparison of the mean C_f , C_h , and p_w
- No significant difference is seen between old and new simulations
- The Stanton number values are ≈ 10% higher in the nosetip region
- There is a small difference smaller than 1% in the wall, at $x \approx 0.08$ m
- The skin-friction coefficient for both cases is very similar to the baseflow values
- There is no sign of an increase in the skin-friction or heat transfer coefficient
  - The flow remains laminar at least up to $x = 0.55$ m

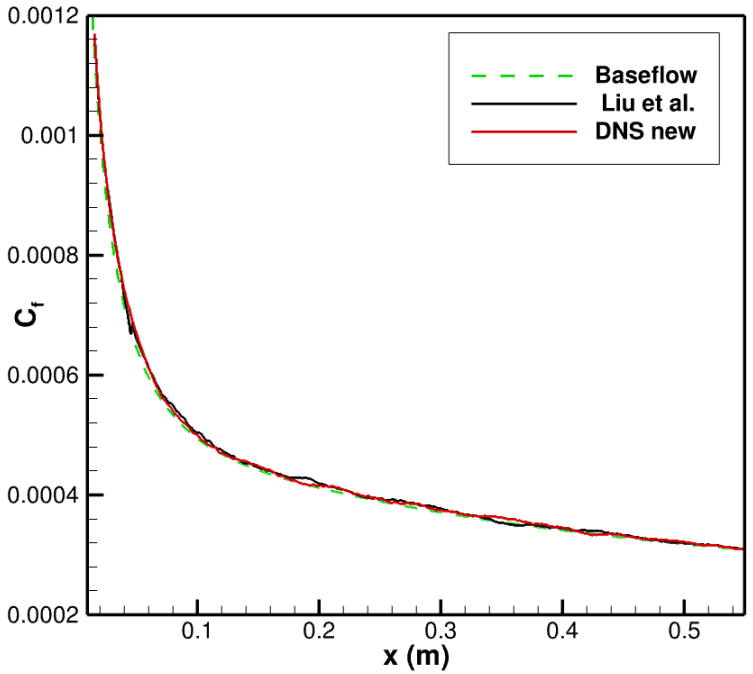

a) Skin friction coefficient C_f

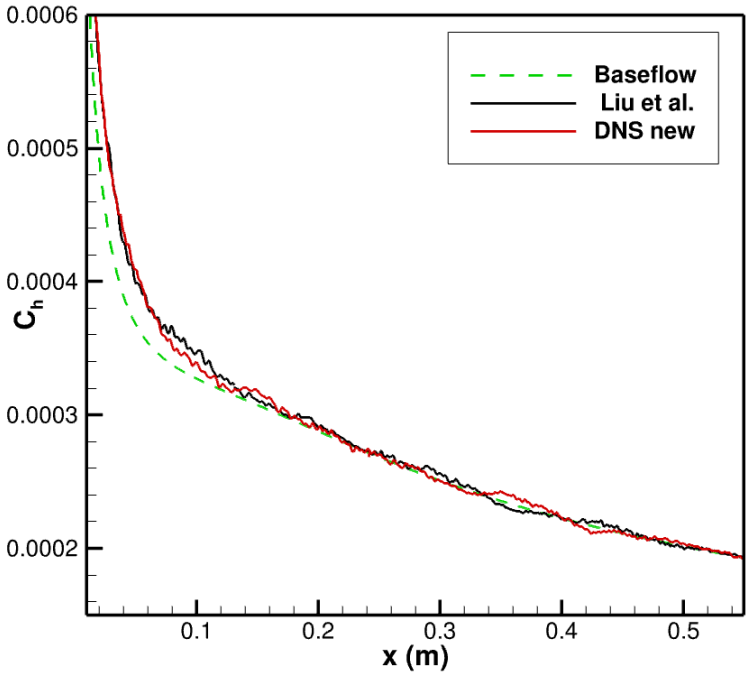

b) Stanton number C_h

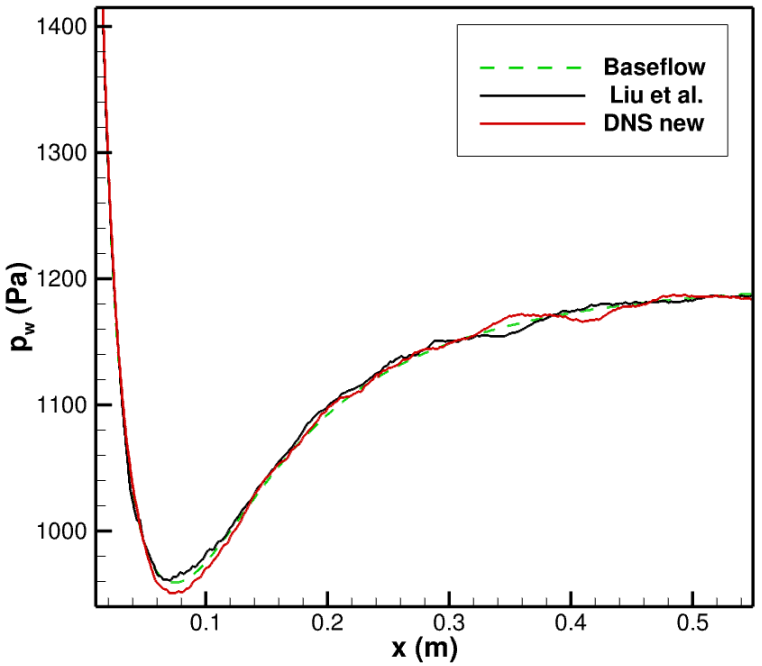

c) Wall pressure p_w

Results: Spectrum Analysis

- Frequency/azimuthal-wavenumber (f-m) spectrum of p'_w and q'_w
- Emergence of a secondary peak at higher frequencies
  - Range of 150 to 200 kHz and m lower than 20
  - A similar high-frequency peak predicted by nonmodal instability analysis (left)
- At the upstream locations, the spectrums are mostly confined to the low frequency and low azimuthal wavenumber
- Secondary peak becomes more evident at downstream locations

Energy gain (nonmodal analysis)

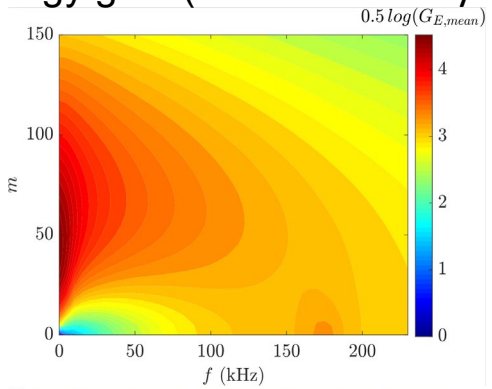

Wall-pressure fluctuation p'_w

Wall heat-flux fluctuation q'_w

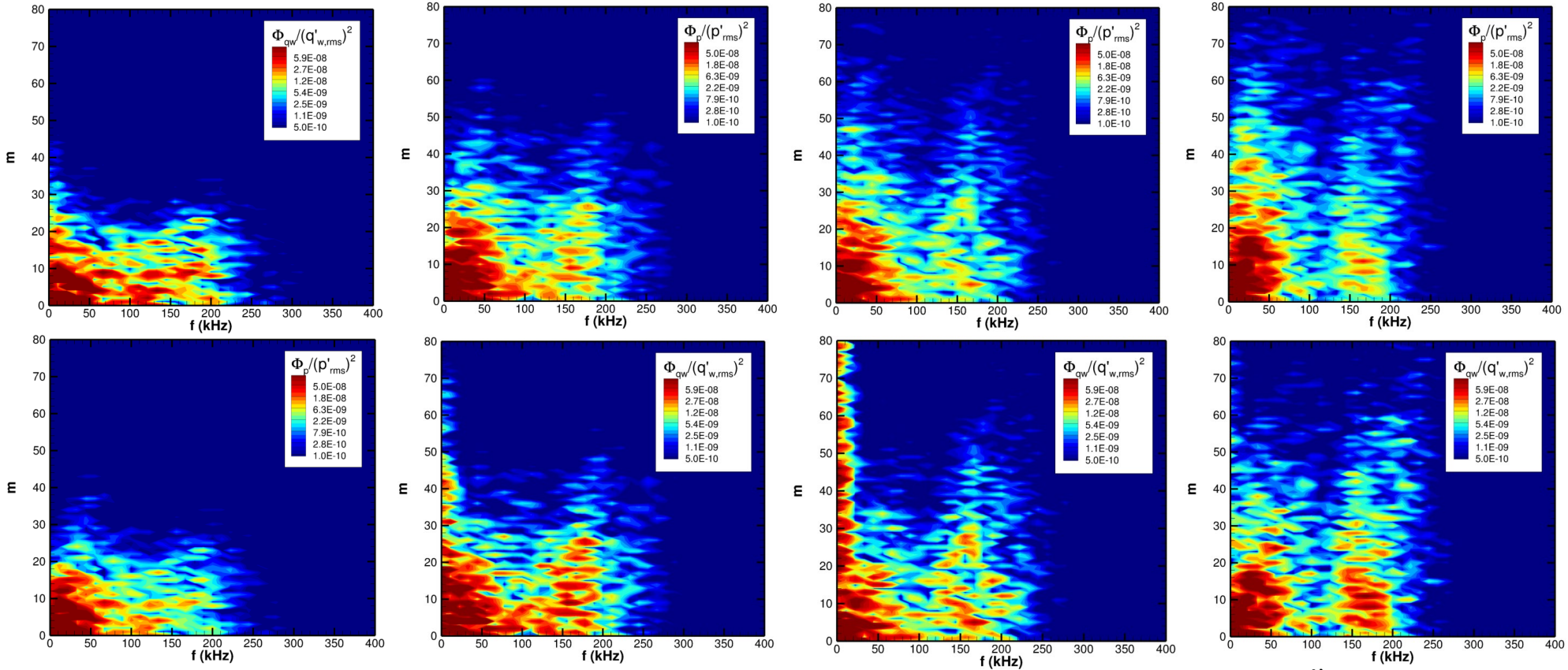

a) x = 0.20m b) x = 0.30m c) x = 0.40m d) x = 0.50m

Results: Spectrum Analysis

- Frequency spectrum of the fluctuations of wall-pressure (p'_w), wall heat-flux (q'_w) and wall skin-friction (τ'_w) as a function of the streamwise coordinate x
- At $x \approx 0.20$ m, the secondary peak between 150 kHz to 200 kHz start appearing
- The peak persists over the entire streamwise domain
  - Nearly constant magnitude
- No super-harmonics of the peak has yet appeared

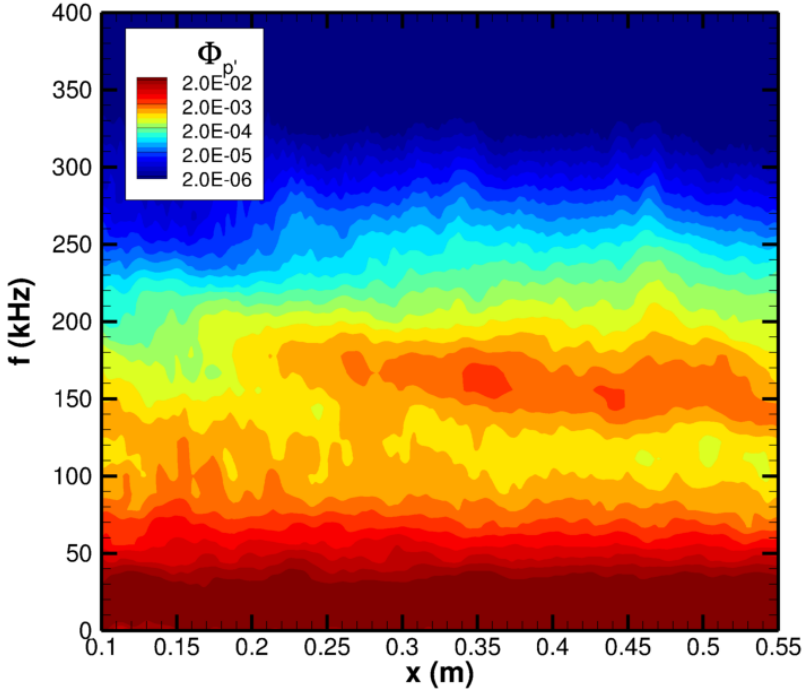

a) Wall pressure p'_w

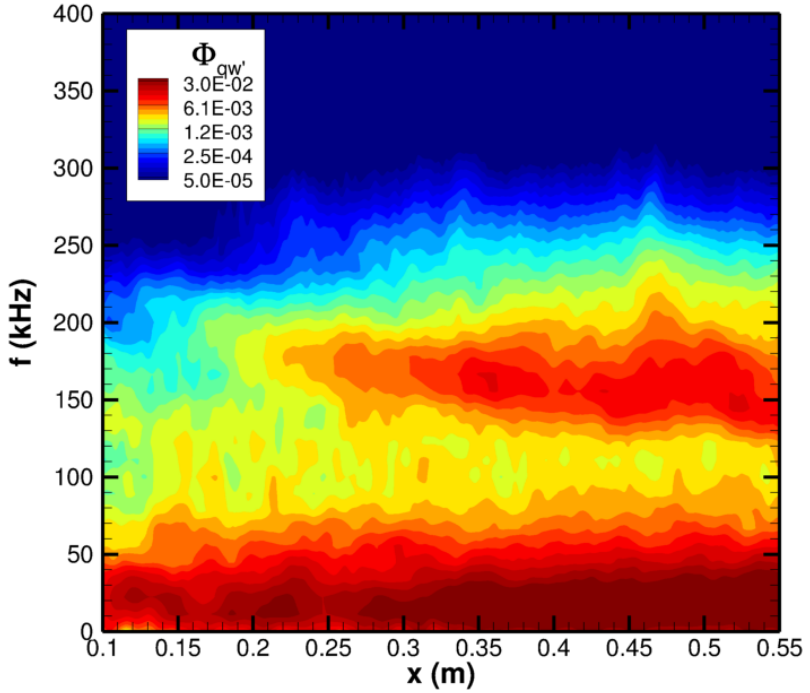

b) Wall heat-flux q'_w

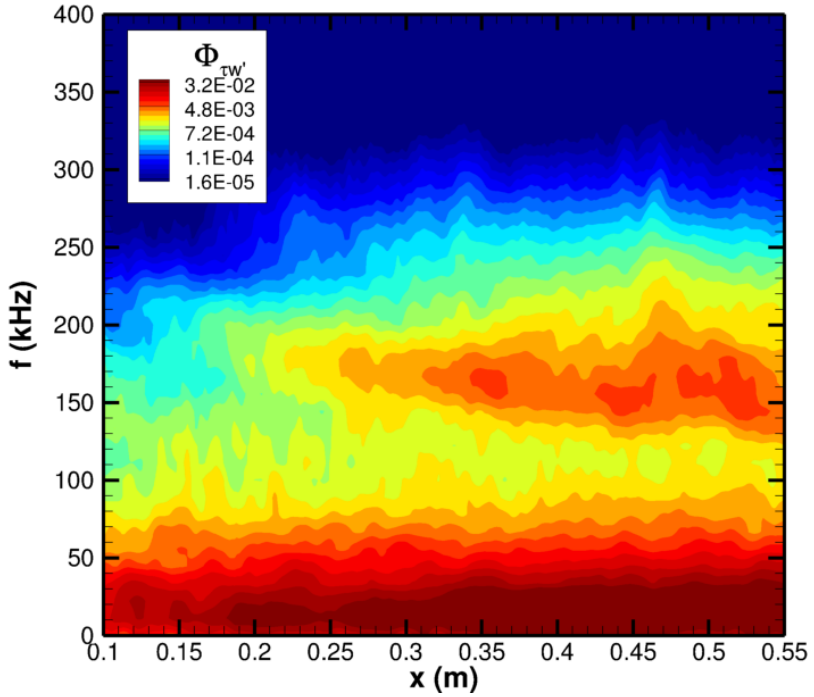

c) Wall skin-friction τ'_w

Results: Spectrum Analysis

- Frequency and azimuthal-wavenumber spectrum of p’ as function of wall-normal distance (z_n)
- The boundary layer acts as a low-pass filter:
  - Only disturbances with small f and m penetrate into the boundary layer
- The same secondary peak can be observed in the near wall region
- It is confined below the sonic line

Entropy layer thickness (δ_s)
Boundary layer thickness (δ_{ht})
Sonic line (δ_M)

Azimuthal wavenumber spectrum of pressure p’

Frequency spectrum of pressure p’

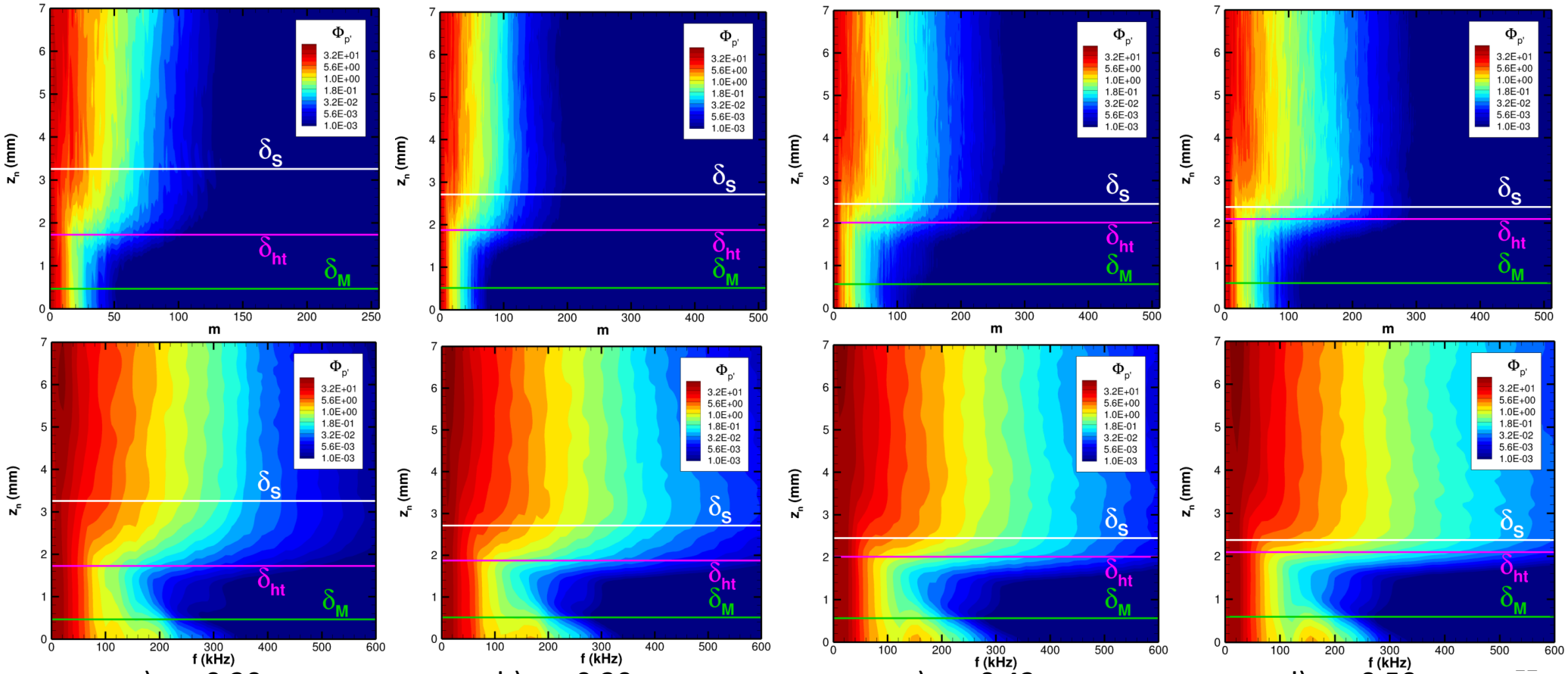

a) x ≈ 0.20 m b) x ≈ 0.30 m c) x = 0.42 m d) x = 0.50 m

Results: Spectrum Analysis

- Frequency and azimuthal-wavenumber spectrum of T’ as function of wall-normal distance (z_n)
- The secondary peak around $f \approx 175$ kHz also appears
  - Confined between the wall and the sonic line
- The frequency spectrum is broader close to the entropy layer edge
- The azimuthal wavenumber spectrum is broader between the δ_{ht} and δ_M
- No additional peak is seen as observed in our previous work [Liu et al. (2022)]

Entropy layer thickness (δ_s)
Boundary layer thickness (δ_{ht})
Sonic line (δ_M)

Azimuthal wavenumber spectrum of temperature T’

Frequency spectrum of temperature T’

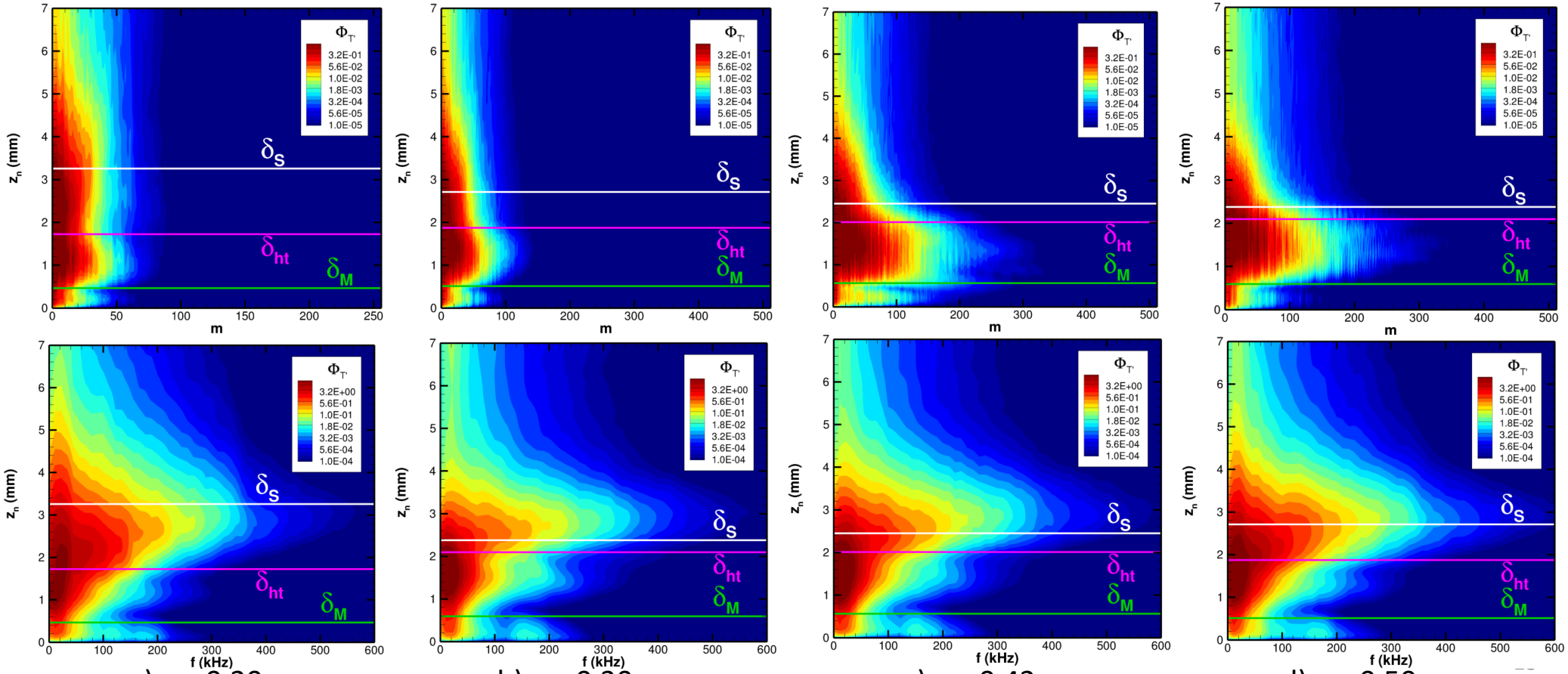

a) x ≈ 0.20 m b) x ≈ 0.30 m c) x = 0.42 m d) x = 0.50 m

Results: Spectrum Analysis

- Frequency and azimuthal-wavenumber spectrum of u’ as function of wall-normal distance (z_n)
- The secondary peak is not too evident as in pressure and temperature fluctuations
- Most of the signal energy is inside the boundary layer
- The wavenumber spectra become broader at further downstream location
- The frequency spectra remain nearly unchanged

Entropy layer thickness (δ_s)
Boundary layer thickness (δ_{ht})
Sonic line (δ_M)

Azimuthal wavenumber spectrum of streamwise velocity u’

Frequency spectrum of streamwise velocity u’

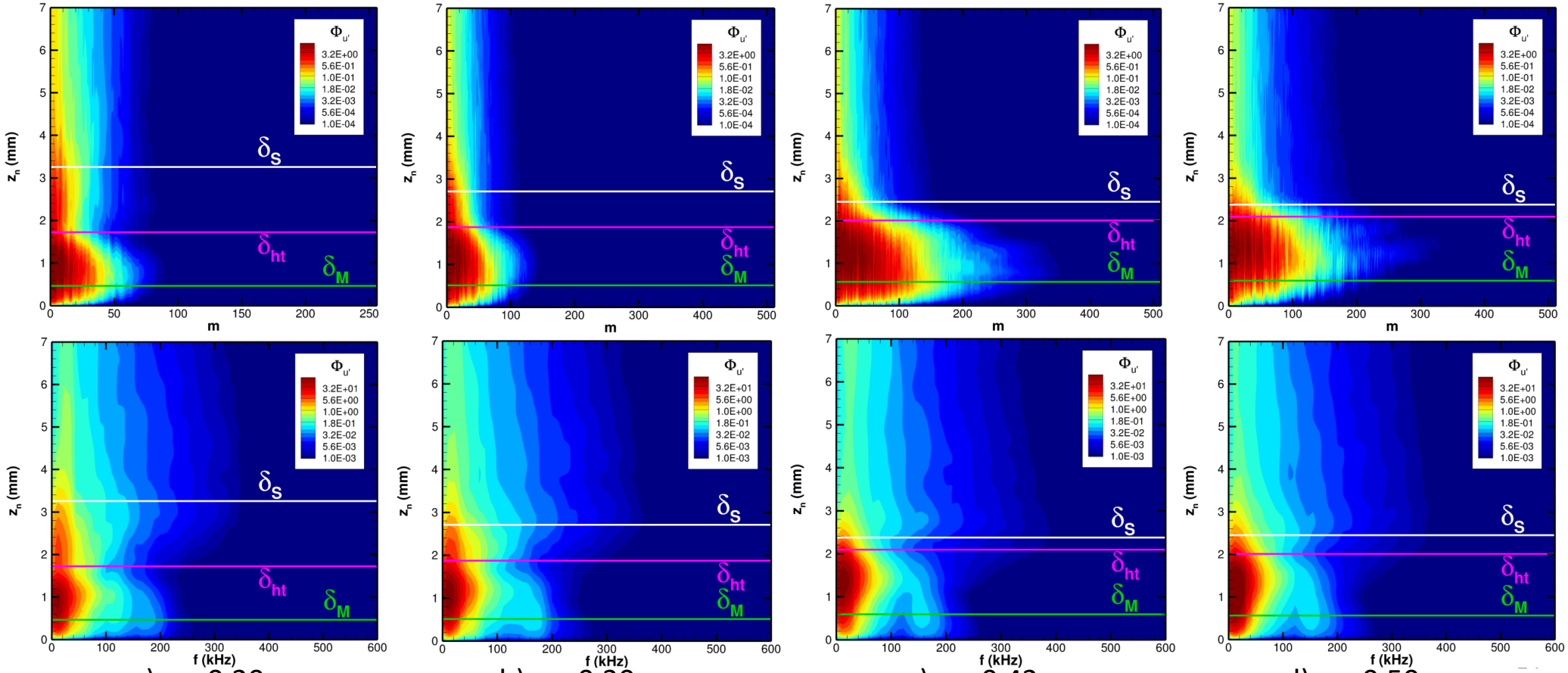

a) x ≈ 0.20 m b) x ≈ 0.30 m c) x = 0.42 m d) x = 0.50 m

Results: Spectrum Analysis

- Fourier mode of the fluctuations for a given frequency and azimuthal wavenumber (f,m) = (177.8 kHz, 0)
- The peak of temperature fluctuation is very close to the edge of the entropy layer (δ_s)
- The peak of pressure fluctuation typically lies above the entropy layer (δ_s)
- A near-wall peak below the sonic line:
  - For pressure, it is exactly at the wall
  - For temperature, it is just above the wall due to the Dirichlet boundary condition for temperature

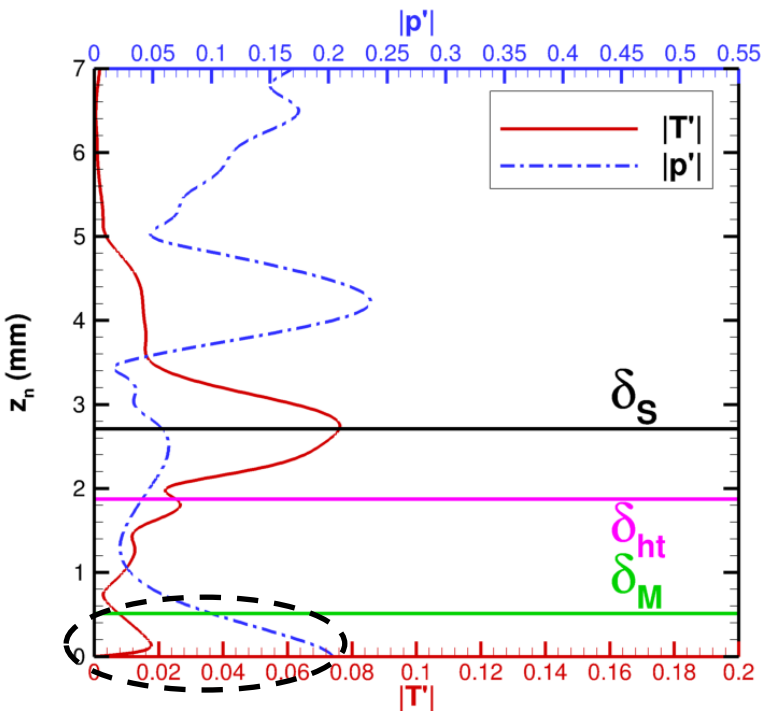

a) x ≈ 0.30 m

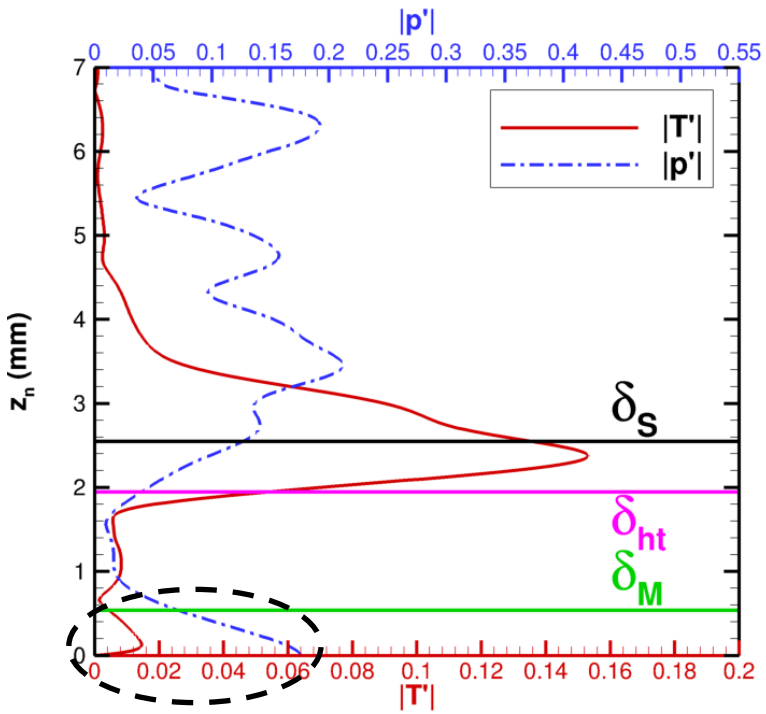

b) x ≈ 0.36 m

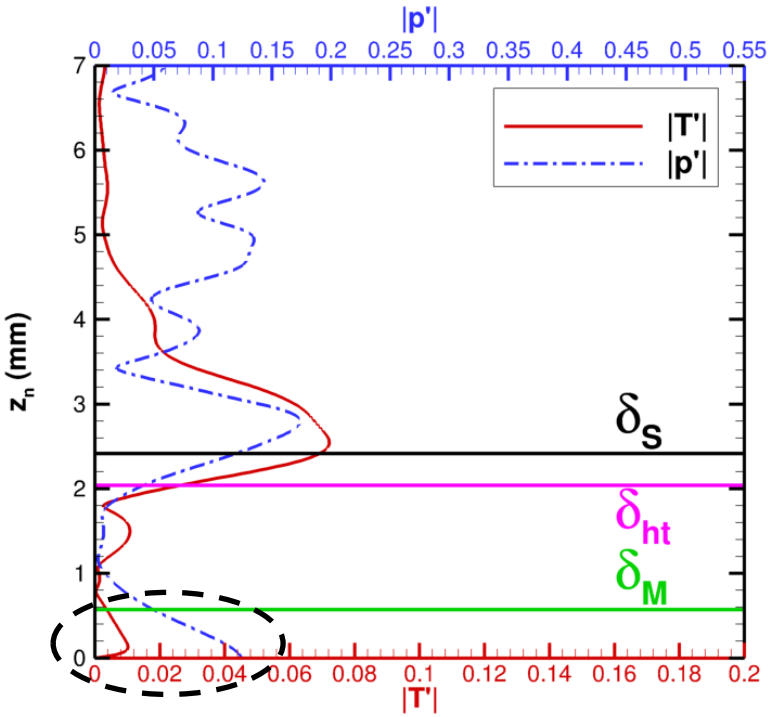

c) x ≈ 0.45 m

Results: Numerical Schlieren Visualizations

- DNS predicts similar inclined structures within the entropy layer as the experimental schlieren measurements (left)
  - These inclined structures may be associated with nonmodal amplifications
  - Structures initially located farther from the wall and approach the boundary layer edge as they travel downstream

Experimental schlieren

7-deg blunt cone with R_n = 4.75 mm in the von Kármán Institute Longshot Hypersonic Wind Tunnel at M = 11.9 (extracted from Grossir et al. 2014)

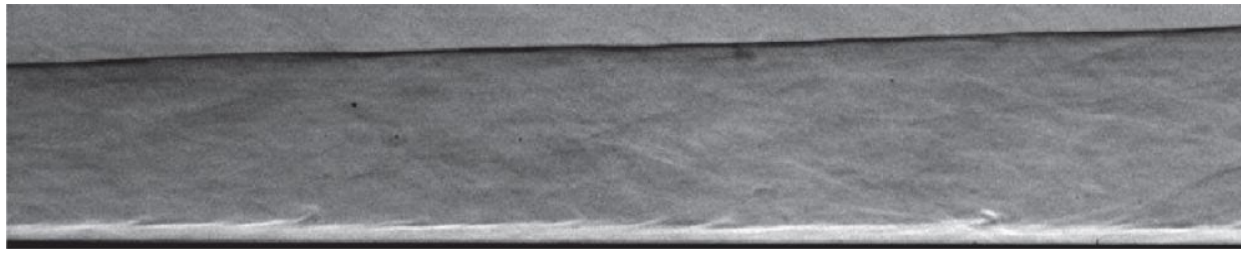

Numerical schlieren predicted by DNS

(7-deg blunt cone with R_n = 5.2 mm in the Sandia Hypersonic Wind Tunnel at M = 8)

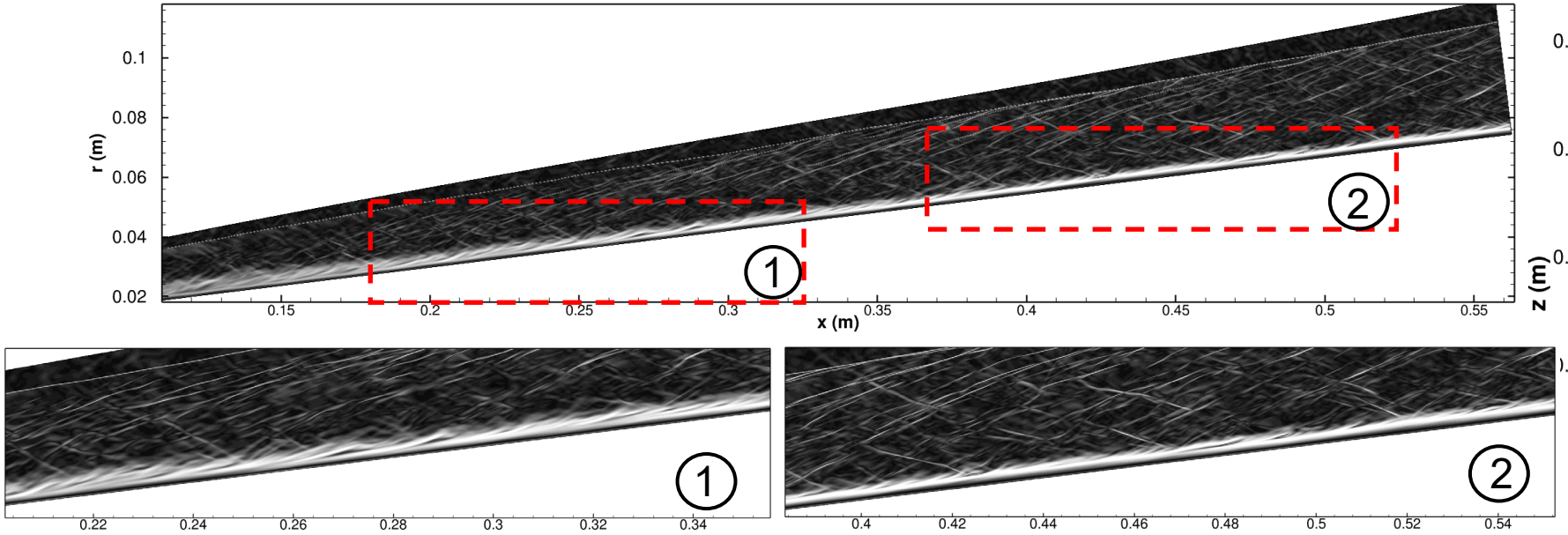

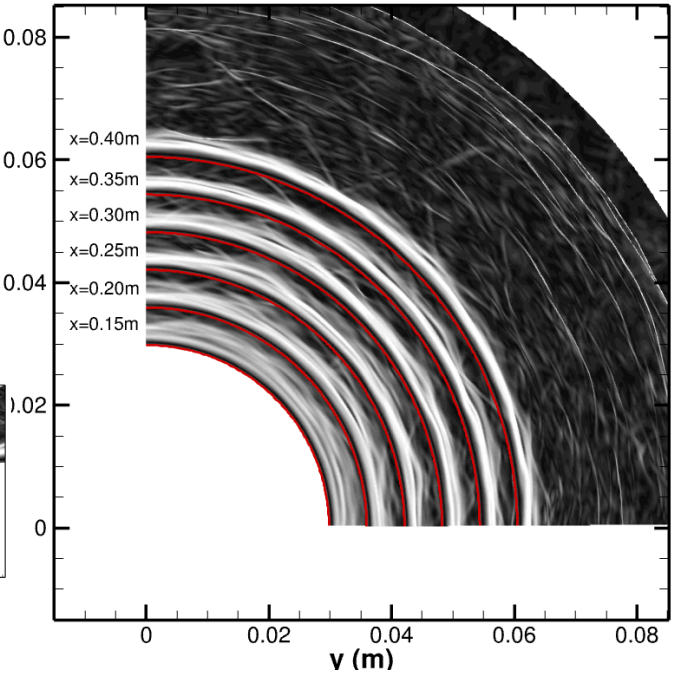

Results: Numerical Schlieren Visualizations

- Temporal/spatial evolution of the numerical schlieren contours showed inclined structures similar to previous experiments
  - Similar inclined structures do not appear for sharp cones (Kennedy et al. 2022)
  - Likely excited by the presence of an entropy layer due to the blunt nosetip
- Cone structures convect with boundary-layer edge speed (i.e., $U_c \approx U_e$)

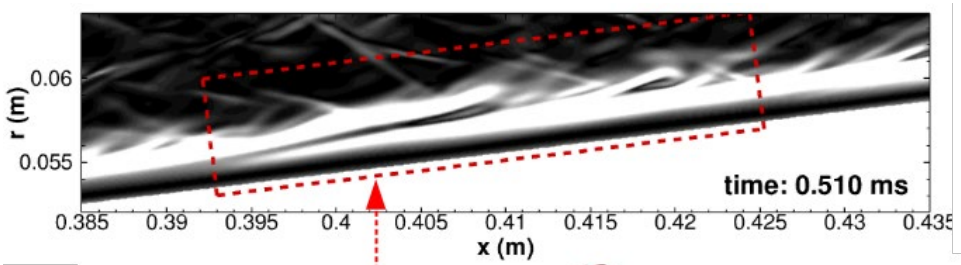

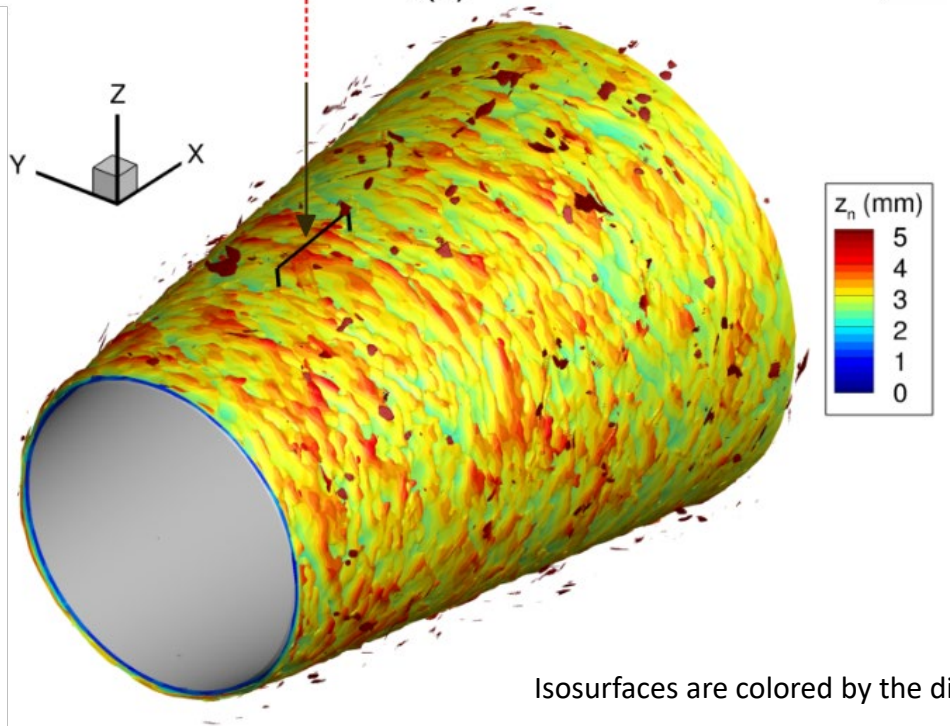

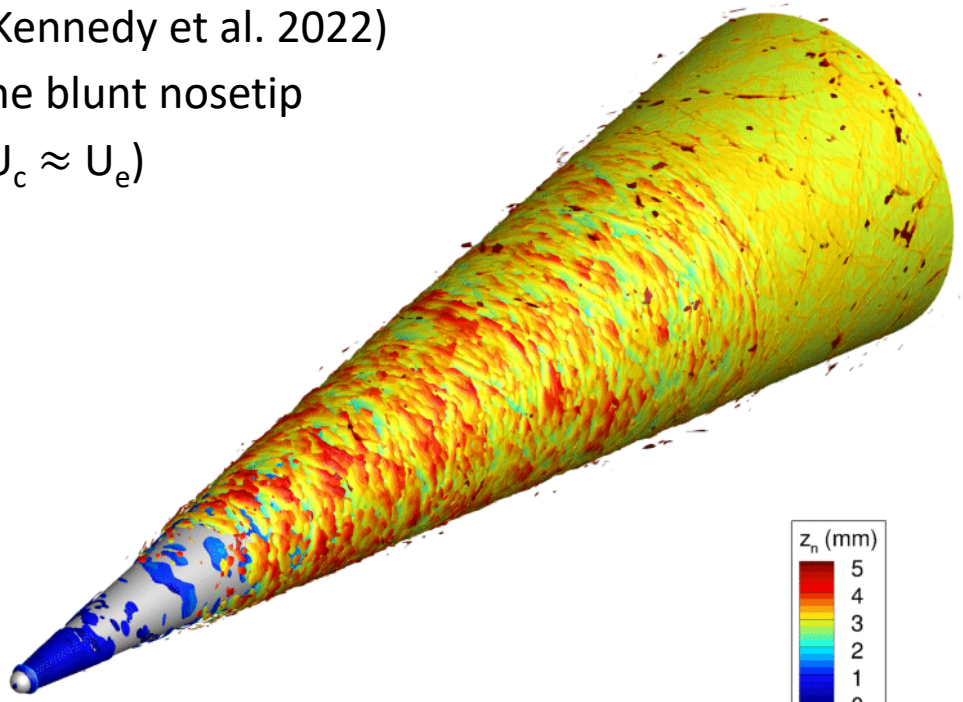

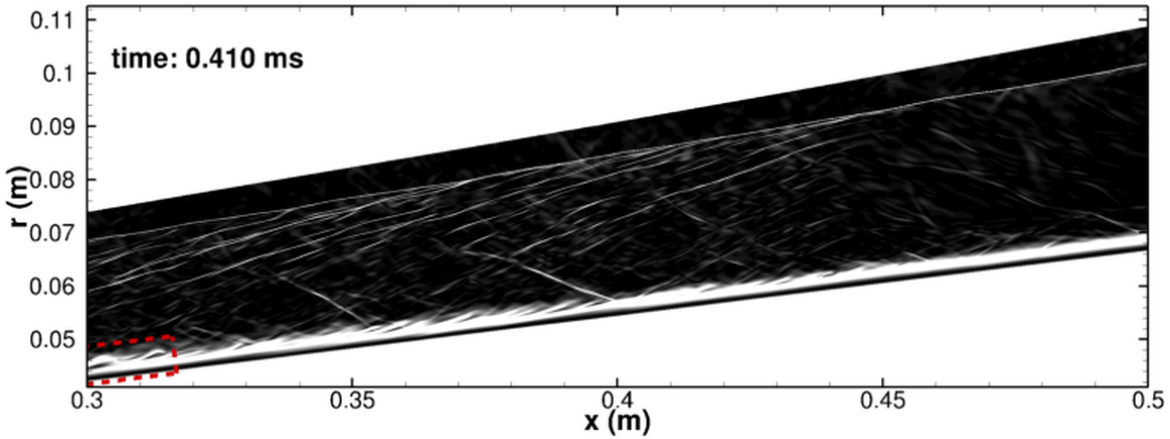

Isosurfaces are colored by the dimensional wall-normal distance

Summary and Conclusion

- Hypersonic boundary-layer receptivity to a freestream acoustic disturbance was investigated using DNS
- The imposed freestream disturbances are based on a Mach 8 digital wind
- Most of the signal energy at the wall is confined to small frequencies and small wavenumbers
- An additional peak of energy between frequencies 150 kHz and 200 kHz
  - This peak agrees well with the predictions of the nonmodal instability analysis
  - Its emergence occurs at $x \approx 0.2$ m
  - Amplitude remains nearly constant along the cone length
- Frequency spectra for temperature fluctuations show a very broadband signal around the entropy layer edge
- As the entropy layer is swallowed by the boundary layer, broader spectra are observed within the boundary layer
- The flow is laminar at least up to $x = 0.55$ m
  - There is no increase in the skin-friction and heat transfer coefficiensts
- The numerical schlieren contours show the same inclined structures observed in the experiments

- Future work will include DNS runs for even longer periods of time and locations further downstream of the cone
  - Try to capture the final breakdown stages of the laminar-turbulent transition

Acknowledgment

- Financial Support
  - ONR
- Computational resources
  - DoD High Performance Computing Modernization Program
  - Ohio Supercomputer Center
  - Argonne Leadership Computing Facility

Hypersonic Boundary-Layer Transition over a Blunt Circular Cone in a Mach 8 Digital Wind Tunnel

Mateus Schuabb, and **Lian Duan**
The Ohio State University, Columbus, OH 43210
Anton Scholten
North Carolina State University, Raleigh, NC 27695
Pedro Paredes
National Institute of Aerospace, Hampton, VA 23666
Meelan M. Choudhari
NASA Langley Research Center, Hampton, VA 23681

Supported by ONR

Backup

Precursor DNS of Full-scale Nozzle of Sandia HWT-8

Visualization of DNS Flowfield

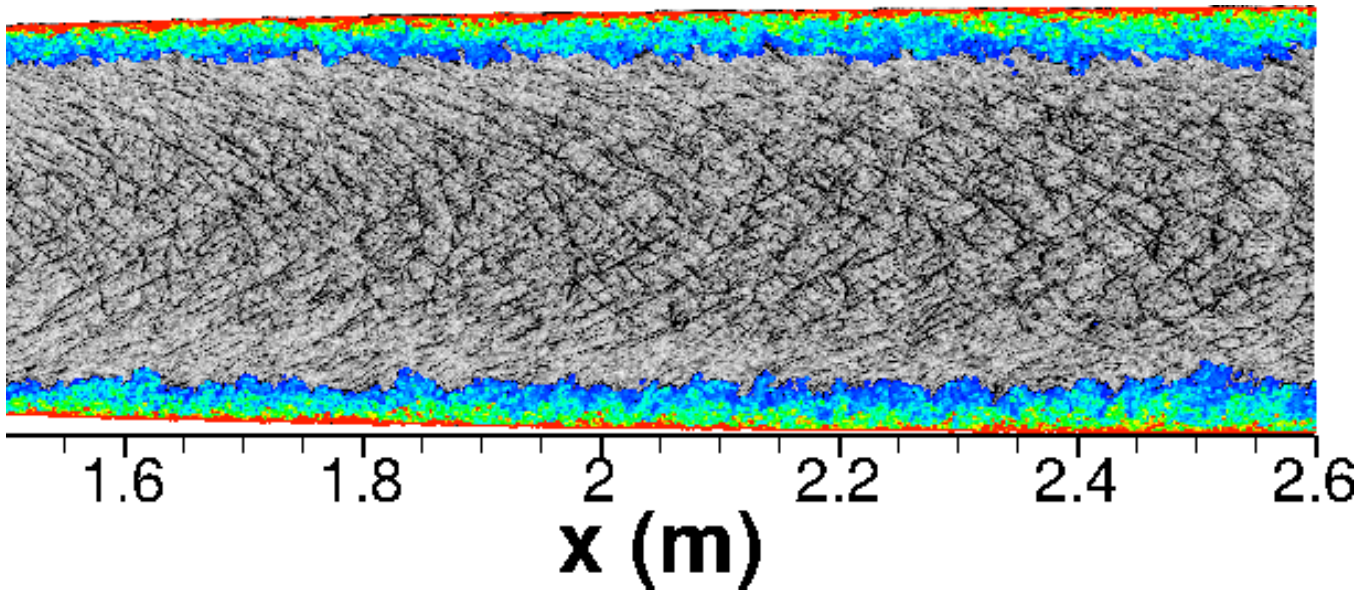

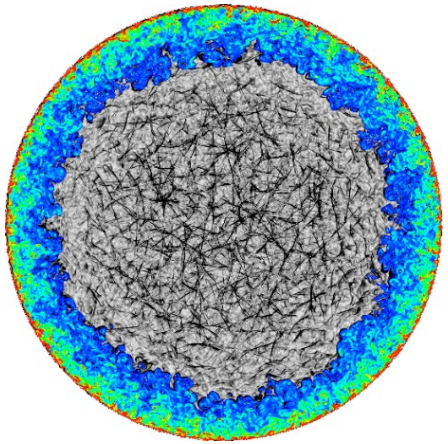

x = 2.336 m

Grayscale: numerical schlieren
Colors: vorticity magnitude

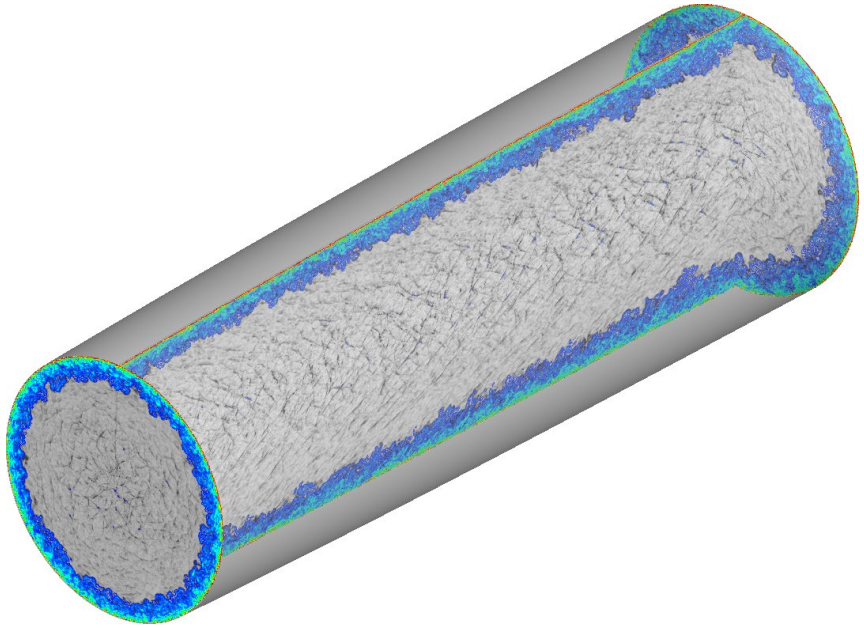

1.5 m < x < 2.6 m

"Tunnel-like" Acoustic Disturbance Generation

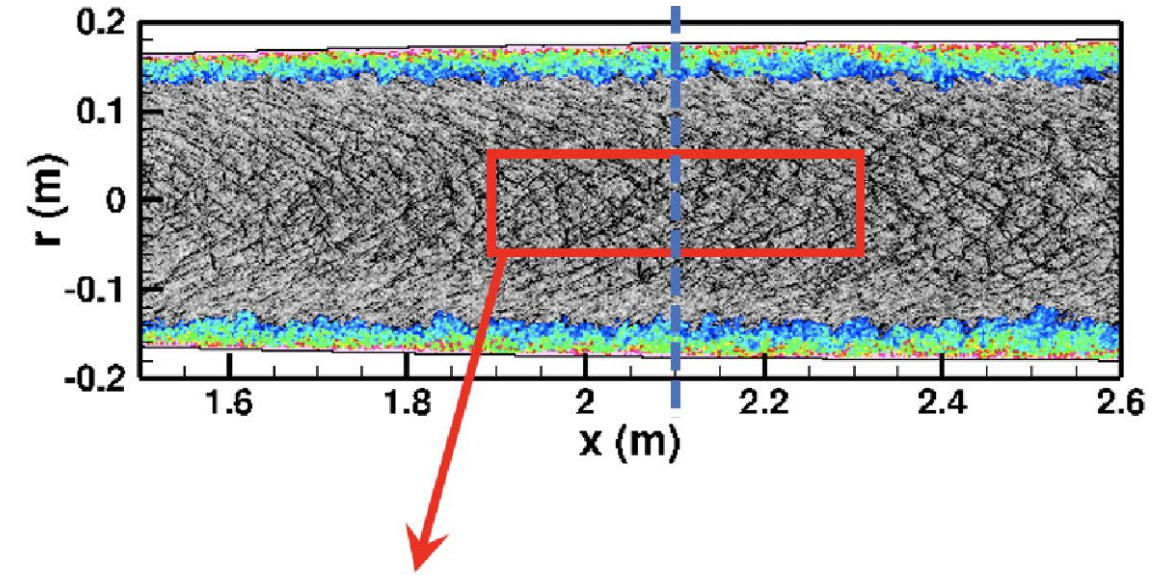

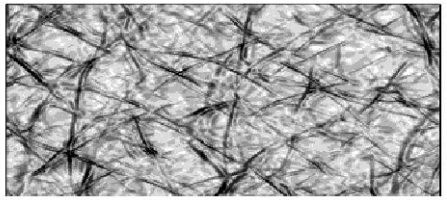

DNS (x-r plane)

extract
reconstruct

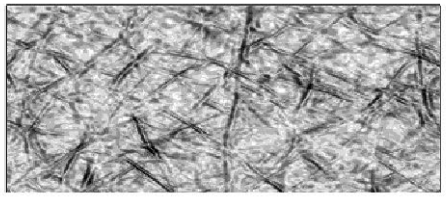

Acoustic Model (x-r plane)

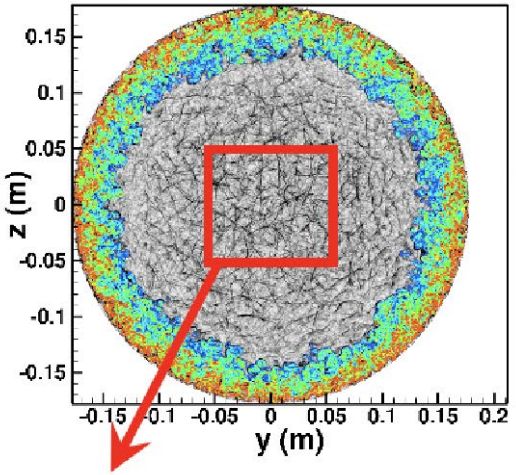

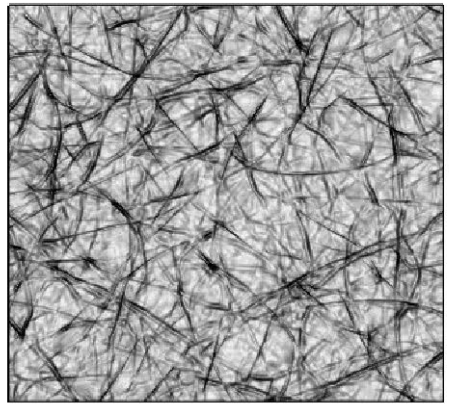

DNS (y-z plane)

extract
reconstruct

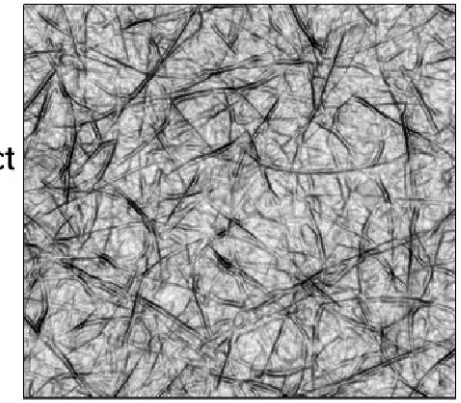

Acoustic Model (y-z plane)

- Instantaneous acoustic structures of the modeled acoustic disturbances matched well with those computed by DNS

"Tunnel-like" Acoustic Disturbance Generation

- "Tunnel-like" acoustic disturbance generation
  - Represent the broadband tunnel noise in the free stream by an acoustic model with an ansatz of plane acoustic waves

$$q'(\boldsymbol{x},t)=\sum_{j=1}^{N}\hat{q}_j\hat{p}_j\left(\boldsymbol{k}_j,\omega\right)e^{-i\left(\boldsymbol{k}_j\cdot\boldsymbol{x}+\omega_j t+\phi_j\right)}+c.c.$$

With $q'=\left(p'_{1,\infty},\rho'_{1,\infty},u'_{1,\infty},v'_{1,\infty},w'_{1,\infty},T'_{1,\infty}\right)^T$

$$\hat{q}_j=\left(1,\frac{1}{\bar{c}_{1,\infty}^2},\frac{1}{\bar{\rho}_{1,\infty}\bar{c}_{1,\infty}}\left(\frac{k_{x,j}}{\|\boldsymbol{k}_j\|}\right),\frac{1}{\bar{\rho}_{1,\infty}\bar{c}_{1,\infty}}\left(\frac{k_{y,j}}{\|\boldsymbol{k}_j\|}\right),\frac{1}{\bar{\rho}_{1,\infty}\bar{c}_{1,\infty}}\left(\frac{k_{z,j}}{\|\boldsymbol{k}_j\|}\right),\frac{(\gamma-1)\bar{T}_{1,\infty}}{\gamma\bar{p}_{1,\infty}}\right)^T$$

  - Apply the dispersion relation for acoustic waves to relate the angular frequency ω_j to wavenumber $\boldsymbol{k}_j$

$$\omega_j=\bar{\boldsymbol{u}}_{1,\infty}\cdot\boldsymbol{k}_j\pm\bar{c}_{1,\infty}\|\boldsymbol{k}_j\|$$

    The plus-minus sign (**±**) indicates that the group velocity of the acoustic waves can be faster or slower than the mean flow velocity
    - "slow" acoustic waves (**-**): $\omega_j=\bar{\boldsymbol{u}}_{1,\infty}\cdot\boldsymbol{k}_j-\bar{c}_{1,\infty}\|\boldsymbol{k}_j\|$
    - "fast" acoustic waves (**+**): $\omega_j=\bar{\boldsymbol{u}}_{1,\infty}\cdot\boldsymbol{k}_j+\bar{c}_{1,\infty}\|\boldsymbol{k}_j\|$
    - The radiated noise from the nozzle-wall turbulent boundary layer dominated by "slow" acoustic waves
  - Calibrate the remaining unknown parameters $\left(\boldsymbol{k}_j,\hat{p}_j,\phi\right)$ in the tunnel noise model using the precursor empty-tunnel DNS data
  - Interpolate the generated acoustic disturbances from the Cartesian domain into the cylindrical domain
    - for the follow-on DNS involving the cone

DNS of Mach 8 Blunt Cone (R_n = 5.2 mm) in a Digital Wind Tunnel

- Frequency/azimuthal-wavenumber (f-m) spectrum of τ'_w
- Emergence of a secondary peak at higher frequencies in the range of 150 to 200 kHz and m lower than 20
  - A similar high-frequency peak predicted by nonmodal instability analysis (left)
- At the upstream locations, the spectrums are mostly confined to the low frequency
- This peak becomes more evident at downstream locations

Energy gain (nonmodal analysis)

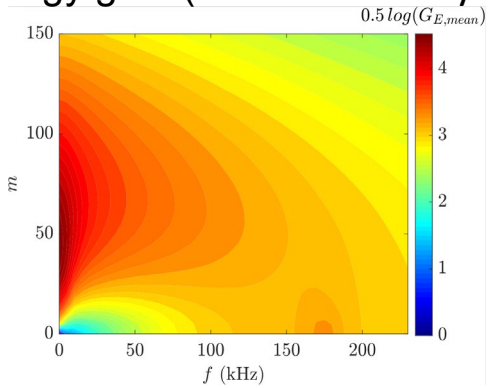

Wall skin-friction fluctuation τ'_w

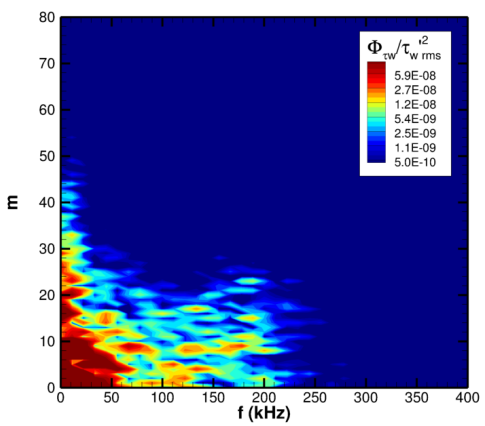

a) x = 0.20m

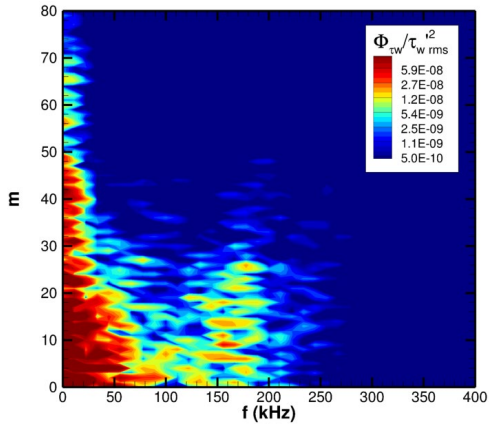

b) x = 0.30m

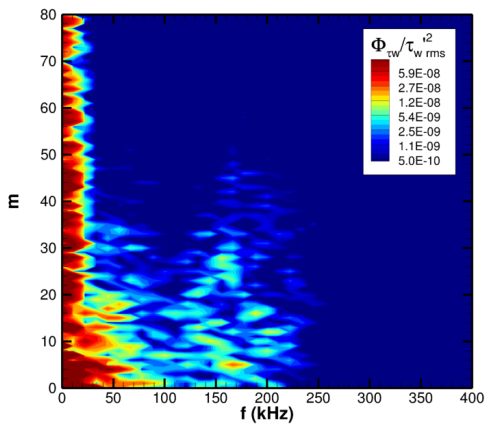

c) x = 0.40m

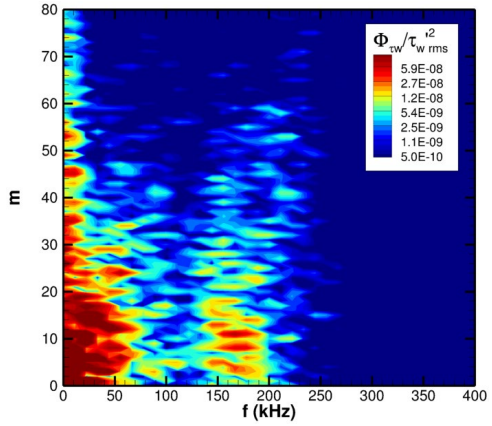

d) x = 0.50m

Results: visualizations

- Temporal/spatial evolution of the numerical schlieren contours
- These inclined structures do not appear for sharp cones [Kennedy et al. 2022], and in our baseflow
  - We suggest they are likely to be excited by freestream acoustic disturbances in the presence of an entropy layer due to the blunt nosetip
- Cone structures convect with a speed approximately equal to the mean flow speed near the boundary-layer edge (i.e., $U_c = U_e$)

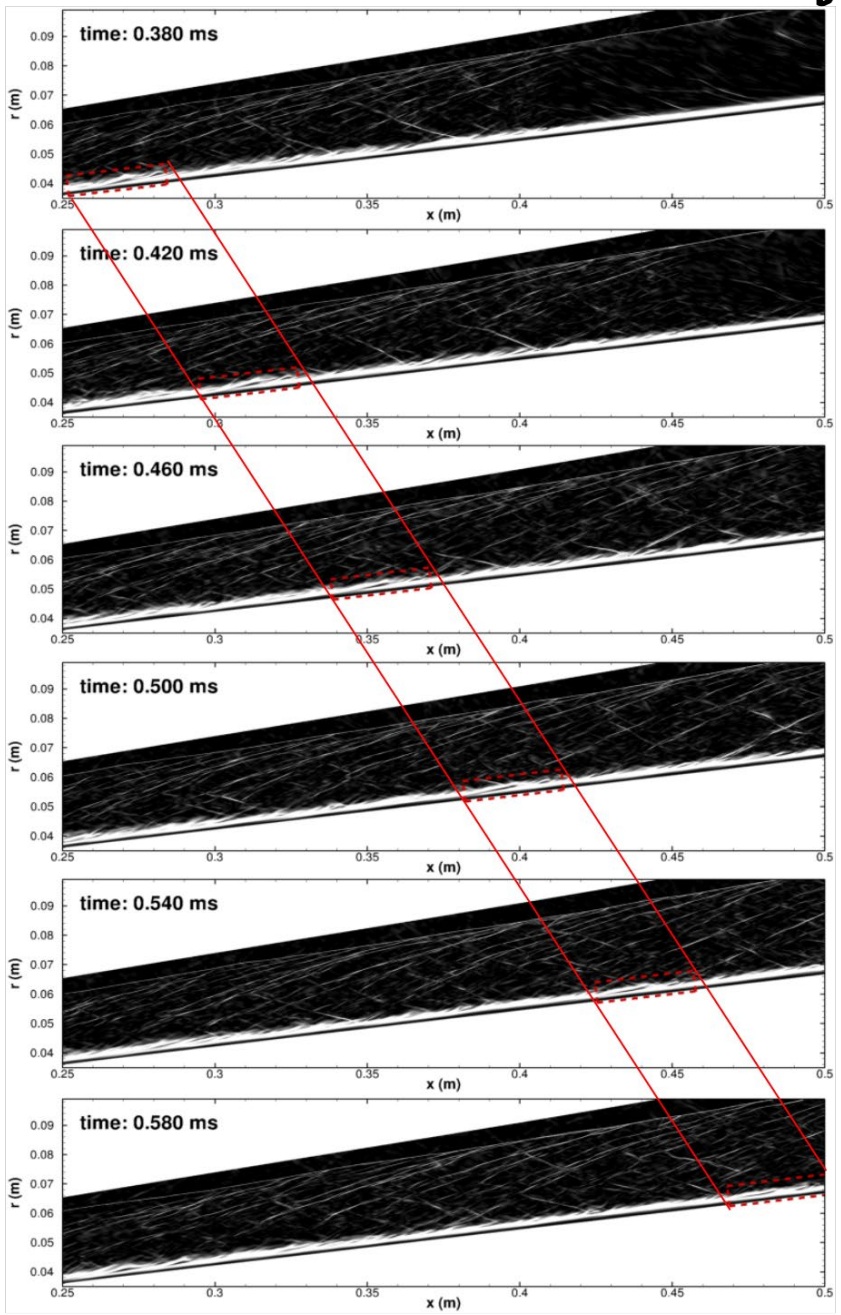

Results: Comparison Between Old and New Results

- Only a qualitative comparison between old and new results
- At transversal planes, it is clear that the transversal oscillations disappear
- The numerical schlieren structures become smoother in the azimuthal direction after the filter

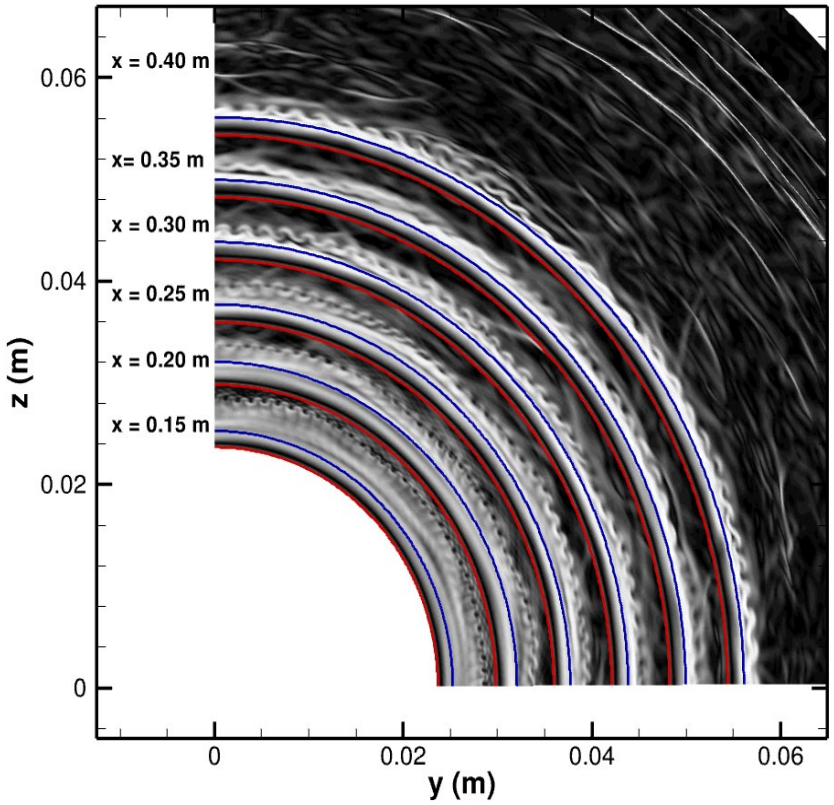

a) Before filter

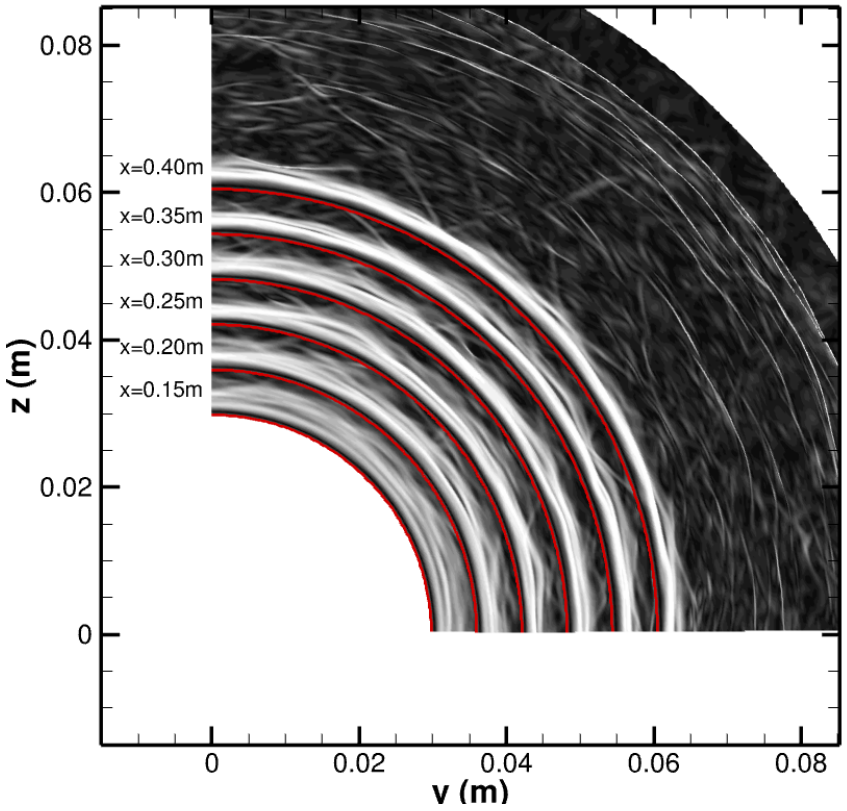

b) After filter

Results: Comparison Between Old and New Results

- Only a qualitative comparison between old and new results
- The inclined structures, at an axial plane, are very similar to the previous results
- They are indeed three-dimensional
  - However, they are free of the spurious periodic azimuthal patterns as observed in the old simulations
  - The azimuthal patterns were indeed caused by numerical noise at the upstream location

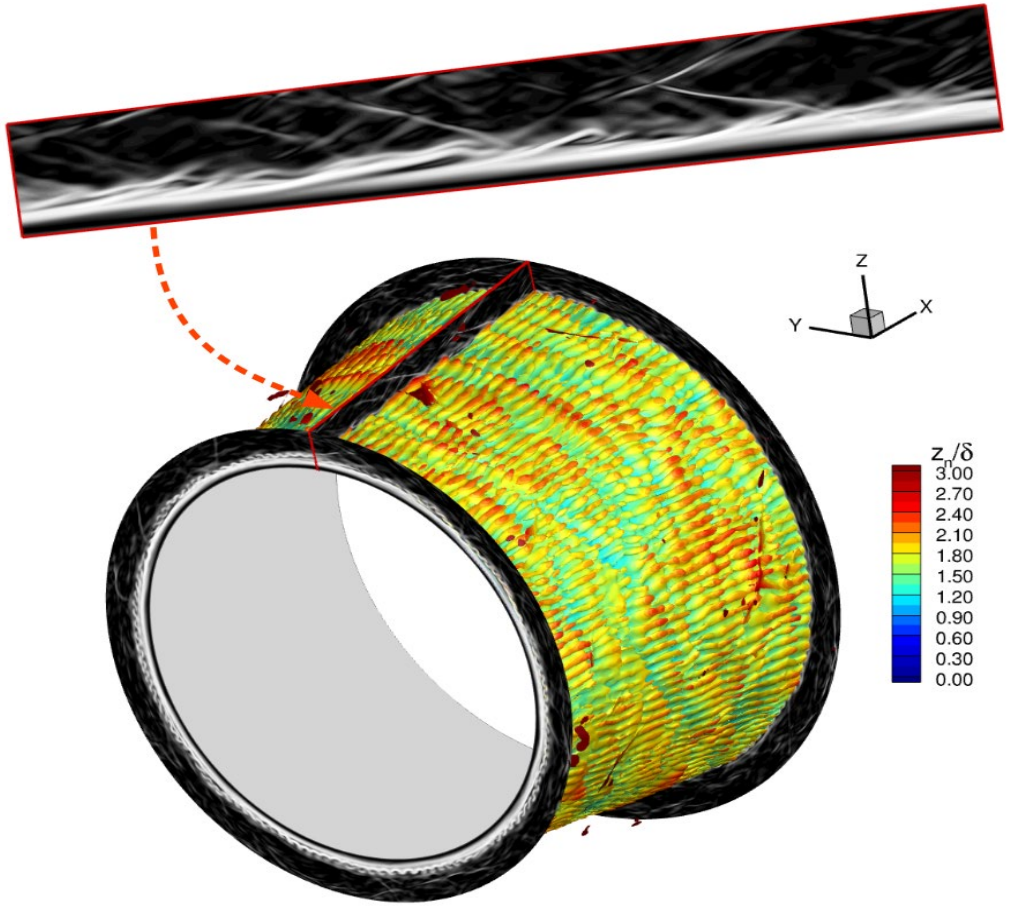

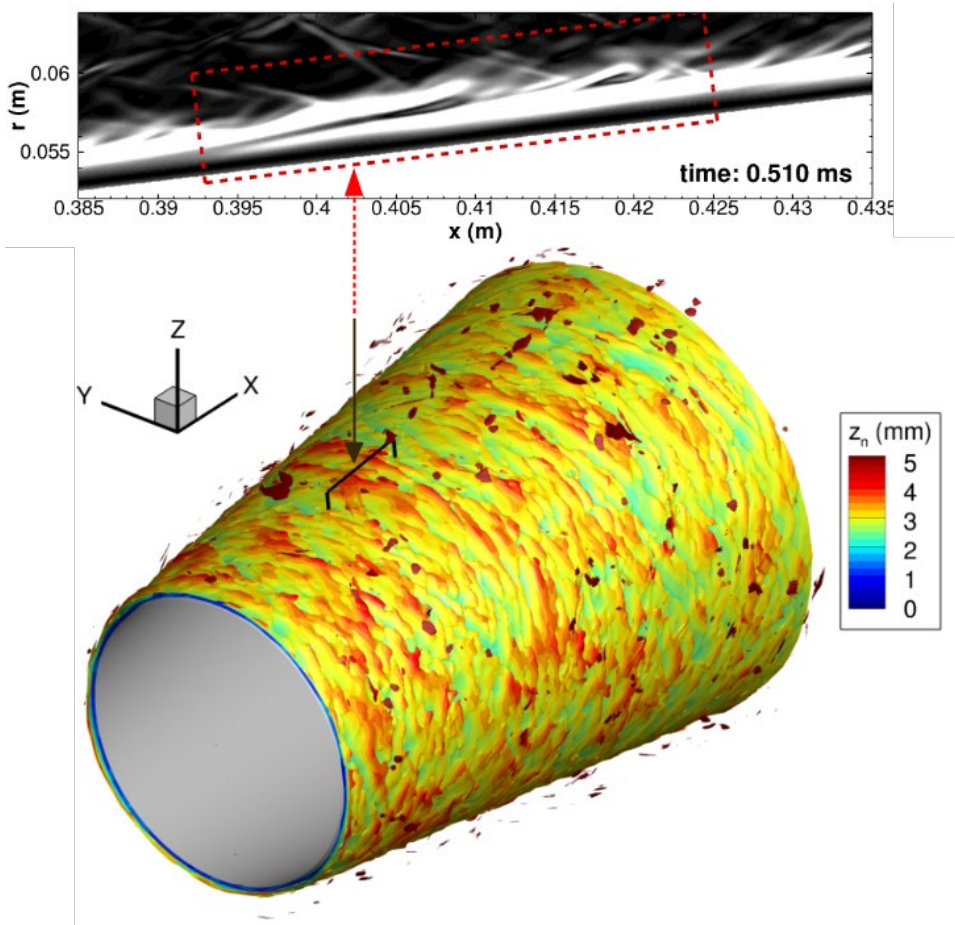

Results: Comparison Between Old and New Results

- A zoomed-in three-dimensional view of such structures

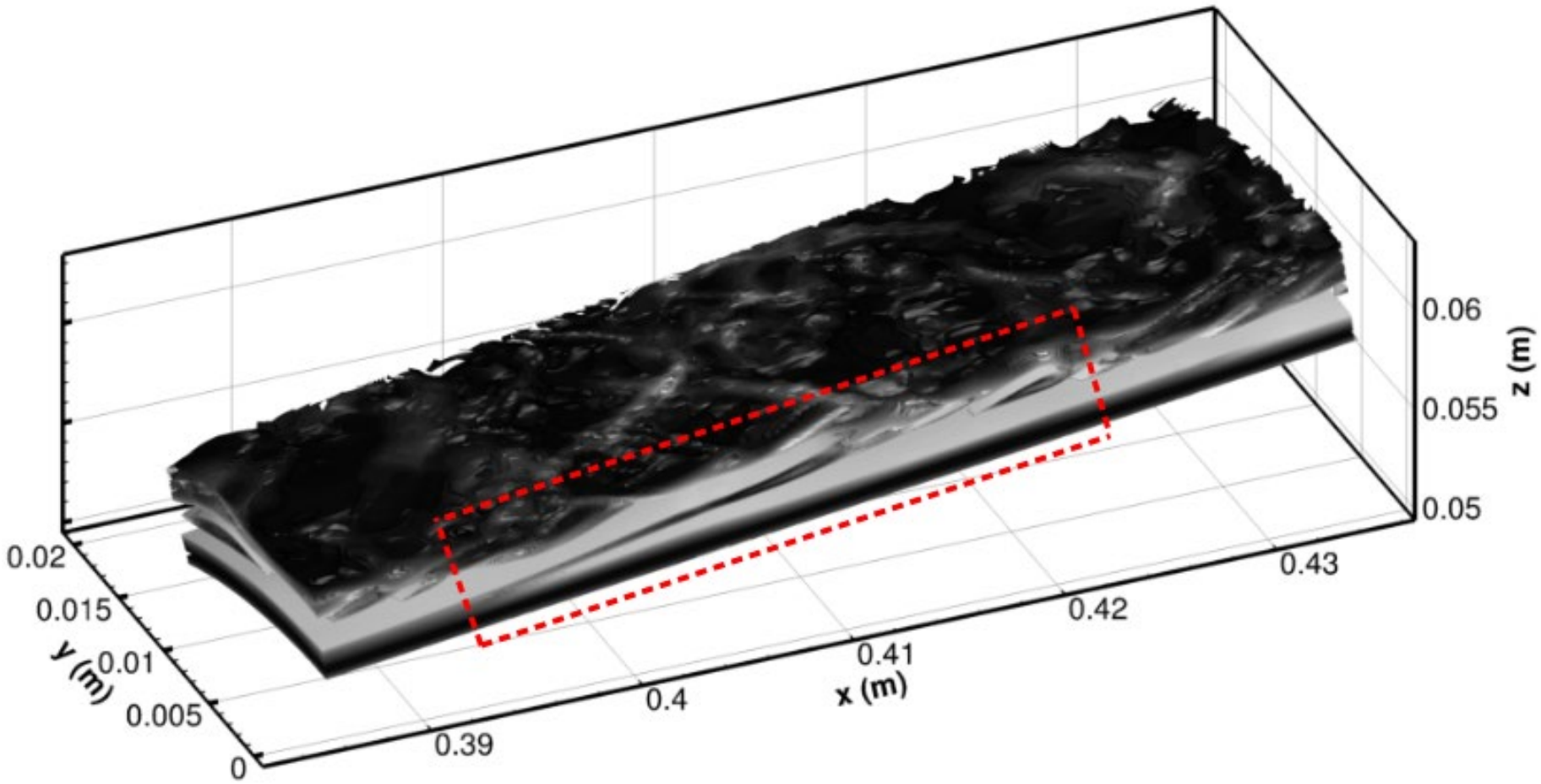

Azimuthal Filtering

- To eliminate the numerical noise, a spectral filter in the azimuthal wavenumber was applied
  - It was used a 4 point-per-wavelength as a cutoff
- Figures below illustrate the comparison before and after the filter for density contours
  - The main structures are maintained
  - The two-point oscillations were vanished

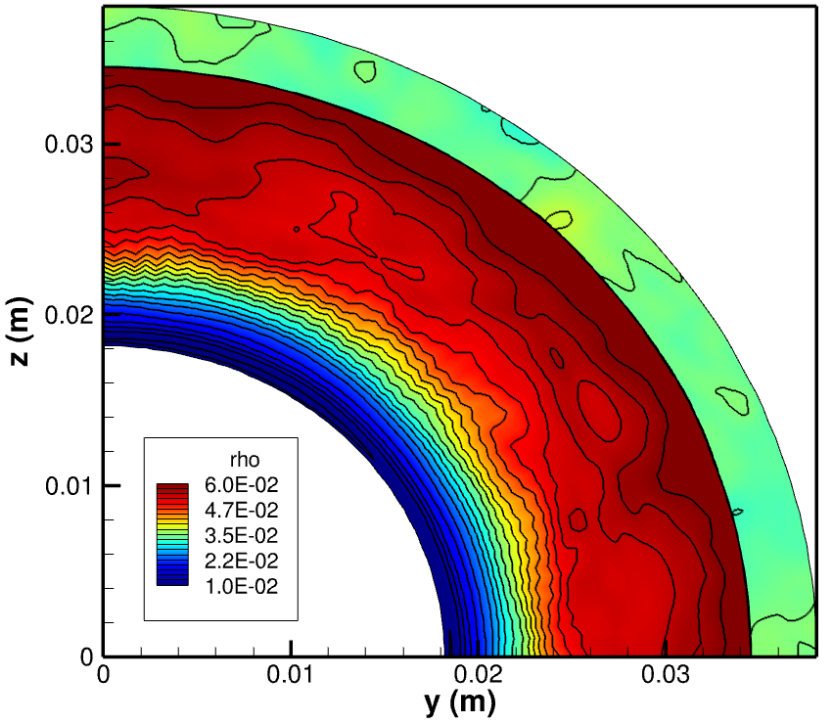

a) Before filter

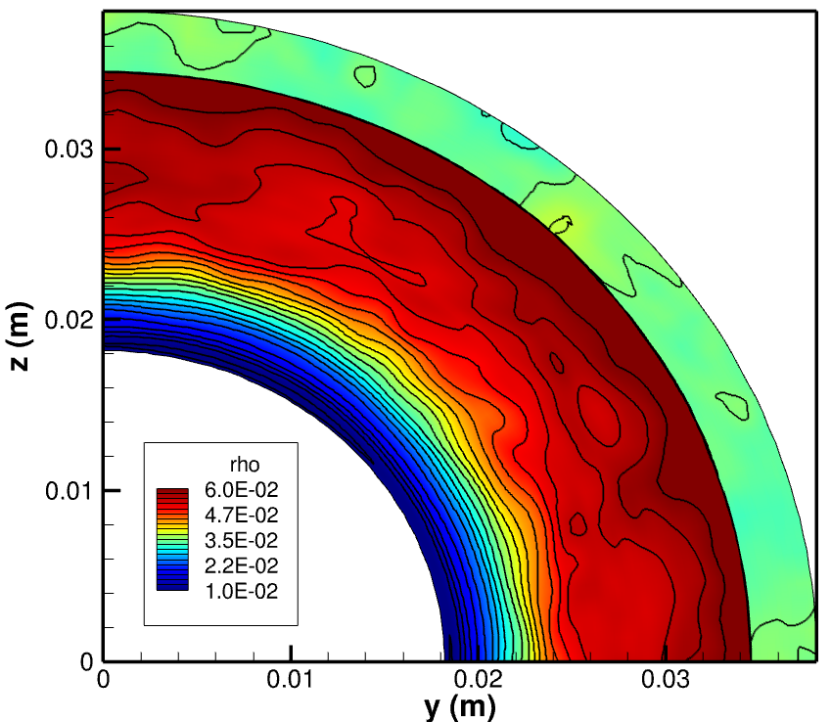

b) After filter

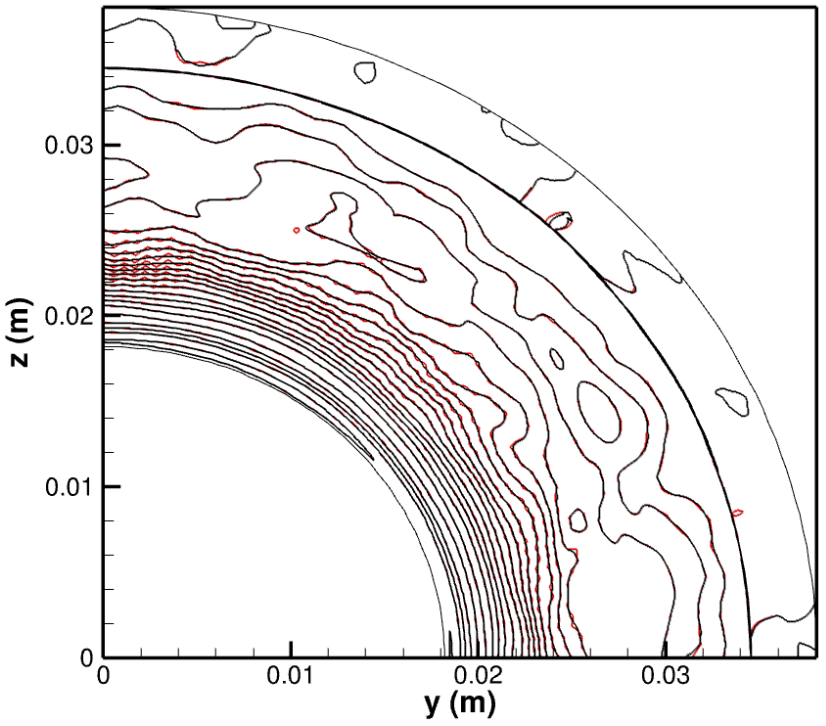

c) Contour line comparison